Evaluating the Cytotoxic Potential of Silver Nanoparticles Derived from Rubus ellipticus against Triple-Negative Breast Cancer

Darakhshan Javaid
Baba Ghulam Shah Badshah University
Shahid Yousuf Ganie
Baba Ghulam Shah Badshah University
Sheikh Showkat Ahmad
Guru Nanak Dev University
Satwinderjeet Kaur
Guru Nanak Dev University
Mohd Salim Reshi
reshisalim@gmail.com

Baba Ghulam Shah Badshah University

Research Article

Keywords: Rubus ellipticus, silver nanoparticles, green synthesis, triple-negative breast cancer, apoptosis

Posted Date: February 27th, 2026

DOI: https://doi.org/10.21203/rs.3.rs-8963159/v1

Additional Declarations: No competing interests reported.

Evaluating the Cytotoxic Potential of Silver Nanoparticles Derived from *Rubus ellipticus* against Triple-Negative Breast Cancer

Darakhshan Javaid[1], Shahid Yousuf Ganie[1], Sheikh Showkat Ahmad[2], Satwinderjeet Kaur[2]
Mohd Salim Reshi[*1]
Corresponding author email: - reshisalim@gmail.com

[1]Toxicology and Pharmacology Laboratory, Department of Zoology, School of Biosciences and Biotechnology, Baba Ghulam Shah Badshah University, Rajouri, Jammu and Kashmir, India-185234

[2]Department of Botanical and Environmental Sciences, Guru Nanak Dev University, Amritsar, Punjab, India- 143005

Abstract

Triple-negative breast cancer (TNBC) is an aggressive and therapeutically challenging subtype of breast cancer, highlighting the need for safer and effective treatment alternatives. Present study was planned to phytofabricate silver nanoparticles using the aqueous leaf extract of *Rubus ellipticus* via an eco-friendly green synthesis approach and to validate their anticancer potential against TNBC. Formation of *Rubus ellipticus* Sm. derived silver nanoparticles (REAgNPs) was confirmed by a visible color change and a characteristic surface plasmon resonance peak at 422nm in UV–Vis spectroscopy. Comprehensive characterization using FTIR, SEM, EDX, TEM, SAED, AFM, XRD and zeta potential analysis revealed stable, spherical, crystalline nanoparticles with an average particle size of 10-30 nm, as determined from TEM measurements. REAgNPs exhibited a potential antioxidant activity in DPPH and hydrogen peroxide scavenging assays. In vitro cytotoxicity studies demonstrated a concentration-dependent antiproliferative effect against MDA-MB-231 TNBC cells, with an IC_{50} value of 30.12µg/mL, comparable to the standard chemotherapeutic drug 5-fluorouracil. Mechanistic investigations revealed that REAgNPs-induced cytotoxicity involved mitochondrial membrane depolarization, nuclear and DNA damage, phosphatidylserine externalization, G0/G1 phase cell cycle arrest and caspase-3 activation, confirming apoptosis via the intrinsic pathway. This study highlights *Rubus ellipticus* derived silver nanoparticles as promising eco-friendly nanotherapeutic candidates for triple-negative breast cancer, warranting further in vivo validation and safety evaluation.

Keywords: *Rubus ellipticus*, silver nanoparticles, green synthesis, triple-negative breast cancer, apoptosis

1. Introduction

Breast cancer is the most frequently diagnosed malignancy among women worldwide and remains a major cause of cancer-related mortality (Wilkinson & Gathani, 2022). Among its subtypes, triple-negative breast cancer (TNBC) is regarded as one of the most aggressive and therapeutically challenging forms, accounting for approximately 15–20% of all breast cancer cases. TNBC is characterised by the absence of oestrogen receptor (ER), progesterone receptor (PR) and Human Epidermal Growth Factor Receptor 2 (HER2) expression, which makes hormonal therapies and HER2-targeted treatments ineffective (Javaid et al., 2025). Clinically, TNBC is associated with high rates of metastasis, early relapse and poor prognosis compared to other breast cancer subtypes. Standard treatment primarily relies on chemotherapy, which often results in systemic toxicity, development of multidrug resistance and compromised quality of life for patients. These limitations have fuelled a search for novel, safer and more effective therapeutic strategies to combat TNBC (Cai et al., 2023).

In recent years, nanotechnology has opened promising avenues for cancer therapy. Nanoparticles, by virtue of their small size, large surface area and unique physicochemical properties, enable enhanced permeability and retention in tumour tissues, improved cellular uptake and the possibility of targeted drug delivery (Chaturvedi et al., 2019; Reshi et al., 2018). Among metallic nanoparticles, silver nanoparticles (AgNPs) have gained significant attention owing to their well-documented antimicrobial, antioxidant, anti-inflammatory and anticancer properties (Dhir et al., 2024; Reshi et al., 2016). The anticancer activity of AgNPs has been linked to multiple mechanisms, including reactive oxygen species (ROS) generation, mitochondrial membrane potential disruption, DNA damage and activation of apoptotic pathways (Shrivastava et al., 2019; Sheikh et al., 2024; Reyaz et al., 2025). Importantly, AgNPs have shown the ability to selectively induce cytotoxicity in cancer cells while sparing normal cells to a certain extent, making them attractive candidates for oncological applications (Wu et al., 2016).

Traditional chemical and physical methods for synthesising AgNPs often require hazardous reducing agents, high energy input and toxic stabilisers, which not only raise environmental concerns but may also compromise the biocompatibility of the final product (Nguyen et al., 2023). In contrast, green synthesis offers an eco-friendly, cost-effective and scalable alternative, employing biological entities such as bacteria, fungi, algae and particularly plants. Plant-mediated nanoparticle synthesis is especially advantageous because plant extracts are rich in diverse phytochemicals such as phenolics, flavonoids, terpenoids, alkaloids, saponins which can act

simultaneously as reducing, capping and stabilising agents (Kirubakaran et al., 2026). Moreover, these phytoconstituents often possess intrinsic biological activities that may synergise with the nanoparticles to enhance their therapeutic potential (Chowdhury et al., 2024).

Medicinal plants with a history of ethnopharmacological use are of particular interest for nanoparticle synthesis, as they offer both chemical diversity and bioactivity (Pattabhiramaiah et al., 2020). *Rubus ellipticus* Sm. (yellow Himalayan raspberry) is a shrub native to the Himalayan region, widely used in traditional medicine for its anti-inflammatory, antimicrobial, antioxidant and antidiabetic properties. Its fruits, leaves and roots contain bioactive compounds such as flavonoids, phenolic acids and tannins, many of which have been reported to exhibit anticancer potential (Sastry et al., 2020). Despite its diverse phytochemical profiles and therapeutic promise, the potential of *Rubus ellipticus* in the green synthesis of AgNPs, especially for anticancer applications, remains largely unexplored. In addition to direct cytotoxicity, oxidative stress modulation is an important factor in the anticancer activity of plant-derived nanoparticles. Antioxidants can influence nanoparticle synthesis efficiency by stabilising the reduced silver nuclei and controlling particle growth. The antioxidant potential of plant extracts can therefore impact both the physicochemical properties and the biological activity of the resulting nanoparticles (Lee et al., 2025).

Considering these aspects, the present work aimed to utilise the plant for the green synthesis of silver nanoparticles. The synthesised AgNPs were subjected to comprehensive characterization. The anticancer potential was further evaluated against MDA-MB-231 TNBC cells.

2. Experimental Procedure and Requirements

2.1. Reagents and Chemical Compounds

Analytical grade chemicals and reagents were utilized throughout this investigation. High-quality commercial kits and reagents were sourced from established vendors such as Sigma-Aldrich (USA), Hi-Media (India), Promega (USA), Invitrogen (USA), Gibco (USA), Central Drug House (India), and Cell Signaling Technology (USA).

2.2. Collection and Taxonomic Authentication of Plant Specimen

Fresh leaves of *Rubus ellipticus* were collected from the main campus of Baba Ghulam Shah Badshah University, Rajouri, Jammu and Kashmir, India, between April and September 2024. Authentication of the plant material was conducted at the Centre for Biodiversity Studies, Baba Ghulam Shah Badshah University, Rajouri, India by Dr. Shreekar Pant.

2.3. Biofabricated Synthesis of Silver Nanoparticles

Bioreduction of silver ions to AgNPs was carried out using the aqueous plant extract based on the method reported by Bindhu and Umadevi (2014), with minor modifications. In Brief, 1 mL of the extract was added to 50 mL of 5 mM silver nitrate ($AgNO_3$) solution. The resulting mixture was incubated at 37 °C for 1 hour in the dark. The biosynthesis of AgNPs was confirmed by a visible color change from pale yellow to reddish-brown. The synthesized nanoparticles were harvested by centrifugation (13,000 rpm, 15 minutes), washed three times with distilled water, and air-dried prior to characterization.

2.4. Physicochemical Evaluation of Biosynthesized AgNPs

2.4.1. Ultraviolet–Visible Spectroscopy (UV–visible spectroscopy)

AgNP formation was confirmed by UV–Vis spectroscopy. A surface plasmon resonance (SPR) peak observed between 300–700 nm verified the reduction of Ag^+ ions and successful synthesis.

2.4.2. Fourier Transform Infrared Spectroscopy (FTIR) Analysis

FTIR analysis of dried AgNPs (mixed with KBr) was conducted using a Perkin Elmer FTIR Spectrum-100 over 4000–400 cm^{-1}. Shifts in absorption bands confirmed the role of phytochemicals in nanoparticle reduction and stabilization.

2.4.3. Scanning Electron Microscopy (SEM) and Energy Dispersive X-ray Spectroscopy (EDX): The morphology and size of AgNPs were examined by SEM. Dried samples were mounted on carbon-coated stubs, sputter-coated, and imaged. Micrographs showed particle shape, surface texture, and aggregation. Elemental composition was determined by EDX, where a strong silver signal confirmed AgNP formation and minor peaks reflected elements from plant biomolecules.

2.4.4. Transmission Electron Microscopy (TEM) and Selected Area Electron Diffraction (SAED) Analysis : The size, morphology, and dispersion of AgNPs were examined by TEM. A drop of nanoparticle suspension was placed on a carbon-coated copper grid and air-dried prior to imaging. High-resolution imaging enabled nanoscale measurement, while SAED patterns with concentric rings confirmed the polycrystalline nature of the nanoparticles.

2.4.5. Atomic Force Microscopy (AFM) Analysis

Particle size distribution and surface morphology of AgNPs were analyzed by AFM using a MultiMode 8 microscope with Nanoscope V controller (Bruker).

2.4.6. X-ray Diffraction (XRD) Analysis

The crystalline structure and phase purity of AgNPs were analyzed by XRD over a 2θ range of 20°–80°. Peaks corresponding to the face-centered cubic (fcc) structure of silver confirmed the formation of crystalline nanoparticles.

2.4.7. Zeta Potential Measurement

The surface charge and colloidal stability of the nanoparticles were evaluated using zeta potential analysis. Measurements were performed in aqueous suspension at room temperature. Negative zeta potential values indicated electrostatic stabilization and good dispersion stability of the nanoparticles.

2.5. Antioxidant Assays

2.5.1 2,2-Diphenyl-1-picrylhydrazyl (DPPH) Radical Scavenging Assay

The DPPH free radical scavenging activity of REAgNPs was evaluated following the protocol of Jadid et al. (2017), with slight adjustments. REAgNPs stock (1 mg/mL) was serially diluted to concentrations of 31.25–1000 µg/mL and mixed with equal volumes of 0.1 mM DPPH solution. After 30 min of dark incubation at room temperature, absorbance was recorded at 517 nm against a DPPH–methanol control. All assays were conducted in triplicate, and scavenging activity was calculated using the equation below:

$$\textbf{Percentage scavenging activity} = \frac{\textbf{Absorbance of control - Absorbance of sample}}{\textbf{Absorbance of control}} \textbf{X 100}$$

2.5.2 Hydrogen Peroxide (H_2O_2) Scavenging Assay

H_2O_2 scavenging by REAgNPs was determined according to Ruch et al. (1989), with modifications. REAgNPs (20–100 µg/mL) were incubated with 40 mM H_2O_2 in phosphate buffer (pH 7.4) at room temperature. Absorbance at 230 nm was recorded against a control (H_2O_2 without REAgNPs). All tests were in triplicate. Scavenging activity (%) was calculated as:

$$\textbf{H}_2\textbf{O}_2 \textbf{ scavenging effect(\%)} = \frac{\textbf{Absorbance of control- Absorbance of sample}}{\textbf{Absorbance of control}} \textbf{X 100}$$

2.6. 3-(4,5-Dimethylthiazol-2-yl)-2,5-Diphenyltetrazolium Bromide (MTT) Assay for Cytotoxicity

Triple Negative Breast Cancer (TNBC) and L929 (normal) cell lines were procured from the National Centre for Cell Science, Pune, India. Cells were cultured in DMEM containing 10% FBS, 1% penicillin–streptomycin, and 1% glutamine, and maintained at 37 °C with 5% CO_2. Cytotoxicity of REAgNPs was evaluated by MTT assay following Siddiqui et al. (2014). Cells seeded in 96-well plates (1×10^4 cells/mL) were treated with REAgNPs (10–100 µg/mL) for 24 and 48 h. After incubation, MTT reagent (5 mg/mL) was added, and absorbance was read at 550 nm using an ELISA plate reader (Biorad-PW41, USA). 5-Fluorouracil served as a positive control. IC_{50} values were determined using GraphPad Prism.

2.7. 4′,6-Diamidino-2-Phenylindole (DAPI) Staining

DAPI staining was performed to evaluate nuclear changes in MDA-MB-231 cells treated with REAgNPs, based on the method of Kerrison and Steinke (2010) with modifications. Cells (1×10^5/well) were seeded on coverslips in 6-well plates and incubated overnight. Following 24 h treatment with REAgNPs at IC_{50} concentration (untreated cells as control), cells were washed with PBS, fixed with 3% paraformaldehyde (10 min), and permeabilized with 0.1% Triton X-100 (5 min). Staining was done with 10 µg/mL DAPI for 15 min in the dark, followed by PBS washes. Coverslips were mounted with Vectashield, and nuclear morphology was examined under a Nikon Eclipse TS2 fluorescence microscope (40×, DAPI filter). The assay was conducted in triplicate with independent cultures.

Rhodamine Staining for Detection of Mitochondrial Dysfunction

Rhodamine 123 staining was used to evaluate mitochondrial dysfunction in REAgNP-treated MDA-MB-231 cells, following Lemasters and Nieminen (1997) with modifications. Cells seeded on coverslips (1×10^5/well) were treated with IC_{50} concentration of REAgNPs for 24 h alongside negative control. After washing with PBS, cells were stained with 20 µM Rhodamine 123 (30 min, 37 °C, dark), washed again, fixed with 4% paraformaldehyde (10 min), and mounted with Vectashield. Imaging was performed using a Nikon Eclipse TS2 fluorescence microscope (40×, Rhodamine 123 filter). All experiments were conducted in triplicate with independent cultures.

2.9. DNA Fragmentation Assay

DNA fragmentation induced by REAgNPs in MDA-MB-231 cells was evaluated following Shashi et al. (2006) with modifications. Cells (4×10^5/10 mm dish) treated with IC_{50} REAgNPs along

side negative control for 24 h were harvested with 0.25% trypsin-EDTA, washed with PBS, and centrifuged (1500 rpm, 5 min, 4 °C). Pellets were resuspended in ice-cold PBS, lysed with Triton Tris-EDTA buffer on ice, and centrifuged to isolate fragmented DNA. The supernatant was treated with RNase A (100 µg/mL) and extracted with phenol:chloroform:isoamyl alcohol (25:24:1). DNA was precipitated using 3 M sodium acetate and 70% ethanol, washed, and dissolved in TE buffer. Samples were run on a 2% agarose gel containing ethidium bromide (0.1 µg/mL) at 10 V/cm. Fragmentation was visualized under UV light and imaged with a Bio-Rad gel documentation system

2.10. Annexin V–FITC/PI Apoptosis Assay

Apoptosis in REAgNP-treated MDA-MB-231 cells was assessed using the Annexin V-FITC/PI apoptosis kit (Thermo Fisher, Invitrogen; Cat. No. V13241). Cells seeded in 6-well plates (4×10^5/well) were treated with IC_{50} REAgNPs along with untreated cells for 24 h. After trypsinization, cells were washed with cold PBS, centrifuged (1500 rpm, 5 min), and resuspended in 1X Annexin-binding buffer at ~1×10^6 cells/mL. Aliquots (100 µL) were stained with 5 µL FITC-Annexin V and 1 µL PI (100 µg/mL) for 15 min at room temperature in the dark. Following addition of 400 µL binding buffer, samples were analyzed immediately by BD Accuri C6 flow cytometry at 530 nm (FITC) and 575 nm (PI). Data were analyzed using BD Accuri software to quantify live, early apoptotic, late apoptotic, and necrotic cells. All experiments were conducted in triplicate with independent cultures.

2.11. Cell Cycle Analysis

Cell cycle progression in REAgNP-treated MDA-MB-231 cells was evaluated by PI staining and flow cytometry (Krishan, 1975, with modifications). Cells (4×10^5/well) treated with IC_{50} REAgNPs for 24 h , with a negative control (no drug) included were harvested, washed with PBS, and fixed in 70% ethanol at 4 °C for 2 h. After centrifugation, cells were incubated with RNase A (100 µg/mL) for 30 min, stained with PI (50 µg/mL) for 30 min in the dark, and analyzed immediately by BD Accuri C6 flow cytometry (10,000 events/sample, FL2 channel). Cell cycle distribution was determined using BD Accuri software. Assays were performed in triplicate with independent cultures.

2.12. Western Blot Analysis of Caspase-3

Western blot analysis was carried out to determine the expression level of the apoptotic marker caspase-3 following a previously described protocol with minor adjustments. MDA-MB-231 cells

were seeded at 4 × 10^5 cells per well in 6-well plates and exposed to REAgNPs at the IC_{50} concentration for 24 h, along with an untreated control. Post-treatment, cells were trypsinized (0.25% trypsin-EDTA), washed with 1× PBS, and centrifuged at 1500 rpm for 5 min at 4 °C. The resulting pellet was resuspended in ice-cold PBS and lysed using Triton-Tris-EDTA (TTE) buffer. Lysates were clarified by centrifugation at 12,000 rpm for 20 min at 4 °C, and protein concentration was determined using the Bradford assay. Equal amounts of protein (50 µg) were denatured in loading buffer, separated on 12% SDS-PAGE, and transferred onto a PVDF membrane by wet transfer. After blocking with 5% albumin in TBS-T, membranes were incubated overnight at 4 °C with primary antibodies against caspase-3 (1:500) and β-actin (1:10,000). Following washing, HRP-linked secondary antibody (1:5000) was applied for 1 h at room temperature. Protein bands were visualized using enhanced chemiluminescence (ECL) and imaged with the ChemiDoc® XRS+ system. Densitometric analysis was performed using ImageJ software, and caspase-3 expression was normalized to β-actin to determine relative fold change compared to control.

2.13. Statistical Analysis

Data were obtained from three independent experiments and expressed as mean ± SD. Statistical analysis was carried out using one-way ANOVA with Tukey's post-hoc test (GraphPad Prism 8). A p-value < 0.05 was regarded as statistically significant.

3. Results and Discussion

3.1. Synthesis and Characterization of Silver Nanoparticles

A visible color change from pale yellow to reddish-brown was observed following incubation of the reaction mixture with silver nitrate, indicating the reduction of Ag^+ ions to Ag^0 nanoparticles and confirming the synthesis of REAgNPs (Figure 1). The UV–Vis spectrum of REAgNPs displayed a characteristic surface plasmon resonance (SPR) band at 422 nm, confirming the formation of spherical silver nanoparticles (Figure 2). The SPR profile indicates a moderate particle size distribution and effective stabilization by phytochemicals present in the *Rubus ellipticus* extract. The SPR band arises from collective oscillation of conduction electrons on the nanoparticle surface, a defining feature of AgNPs (Khurana & Jaggi, 2021). Similar SPR positions have been reported for plant-mediated silver nanoparticles, supporting the successful green synthesis of REAgNPs (Khanal et al.,2022; Rahuman et al., 2022). The stability of the SPR signal further suggests suitability of the nanoparticles for subsequent biological applications.

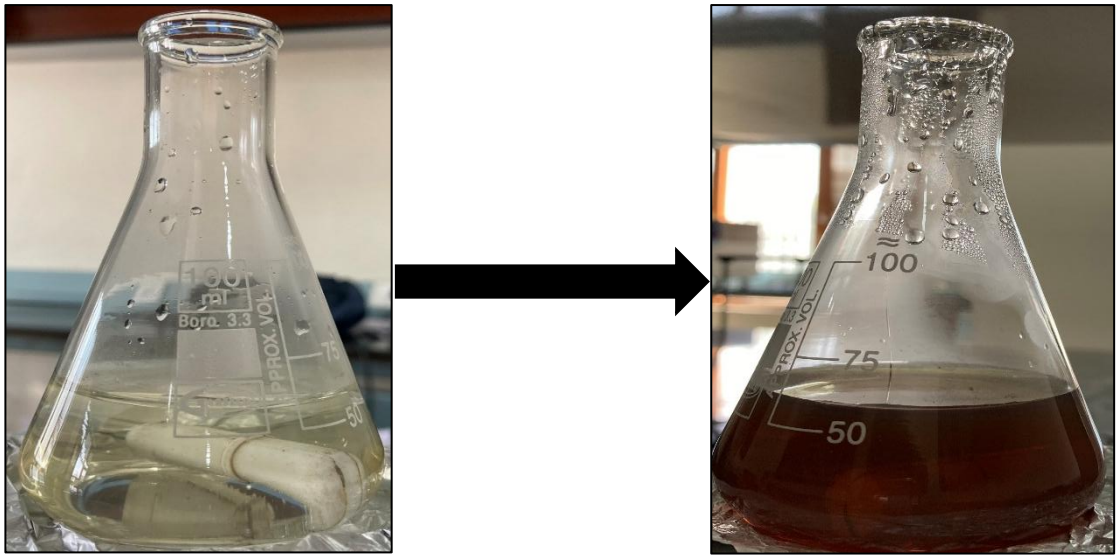

Figure 1. The figure shows the color change of the reaction mixture from pale yellow to dark brown after treatment with *Rubus ellipticus* aqueous extract, indicating the reduction of Ag^{+} ions to silver nanoparticles (AgNPs).

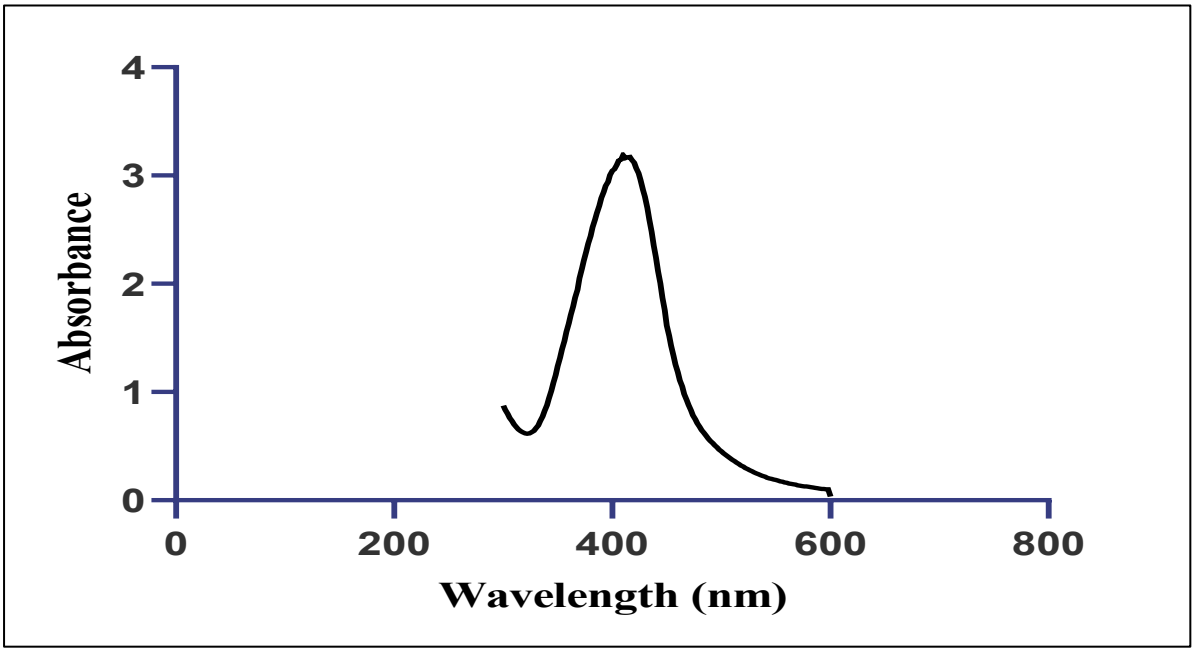

Figure 2. UV-Visible absorption spectrum showing a characteristic SPR peak at 422nm confirming the successful synthesis of silver nanoparticles (AgNPs) using *Rubus ellipticus* aqueous extract.

3.2. FTIR Analysis

FTIR analysis was carried out to identify the functional groups involved in the reduction and stabilization of REAgNPs. The FTIR spectrum (Figure 3) displayed a broad absorption band at 3432 cm^{-1}, corresponding to O–H stretching vibrations of phenolic and alcoholic groups,

indicating the involvement of hydroxyl-containing phytochemicals in nanoparticle formation, consistent with reports from AlQahtani et al., 2024 and Khanal et al., 2022. The peaks at 2926 cm^{-1} and 2854 cm^{-1} were assigned to aliphatic C–H stretching vibrations, suggesting the presence of organic capping agents on the nanoparticle surface. The absorption band at 1634 cm^{-1} is attributed to C=O stretching vibrations of amide or conjugated carbonyl groups, implying the participation of proteins or polyphenolic compounds in nanoparticle stabilization. Bands observed in the region of 1400–1386 cm^{-1} correspond to C–N stretching or O–H bending vibrations of aromatic compounds. Additionally, peaks at 1113 cm^{-1} and 1023 cm^{-1} are characteristic of C–O stretching vibrations of alcohols and polysaccharides, which may contribute to steric stabilization of the nanoparticles. The low-frequency band at ~615 cm^{-1} suggests metal–ligand interactions, confirming the binding of phytochemicals to the silver nanoparticle surface. The FTIR results confirm that biomolecules present in the *Rubus ellipticus* extract functioned as reducing and capping agents, facilitating the green synthesis and stabilization of silver nanoparticles.

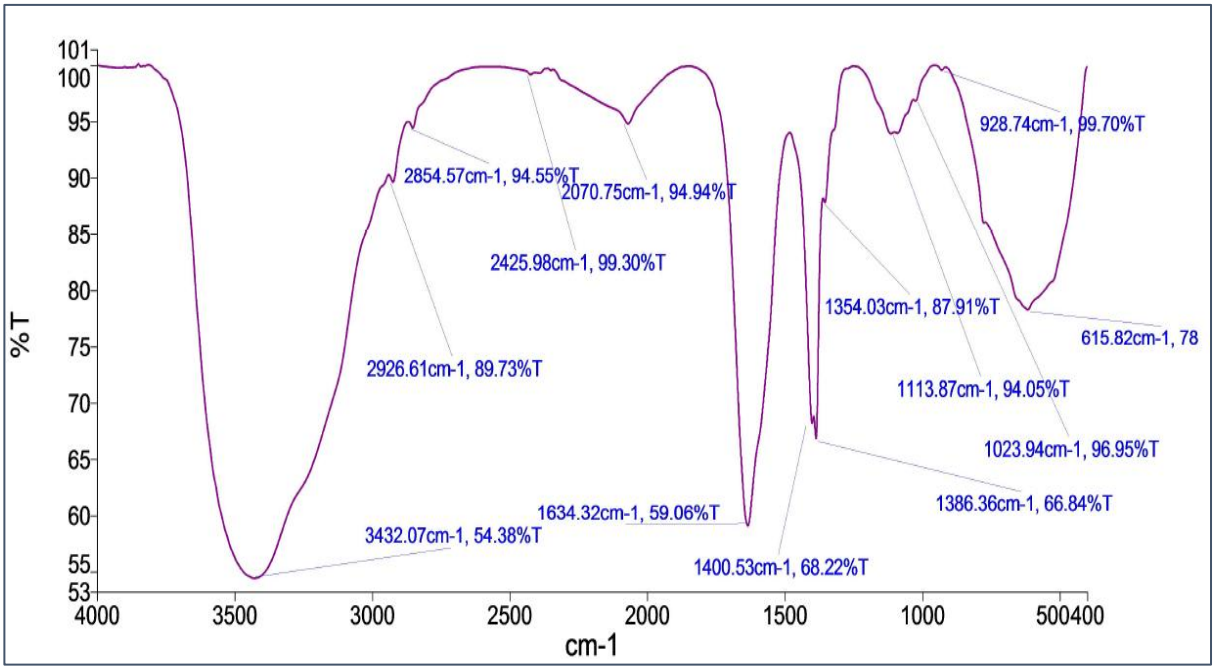

Figure 3. The FT-IR spectra of REA-AgNPs show multiple characteristic absorption bands corresponding to different functional groups derived from plant phytochemicals.

3.3. SEM and EDX Analysis of REAgNPs

Scanning electron microscopy (SEM) was employed to examine the surface morphology of the biosynthesised REAgNPs, while energy-dispersive X-ray (EDX) analysis was performed to confirm their elemental composition. SEM micrographs (Figure 4) revealed that the

nanoparticles were predominantly spherical and existed as densely packed aggregates, indicating successful nanoscale particle formation. Similar spherical morphology and aggregation patterns have been observed in other plant-mediated AgNPs, such as those from *Eclipta alba* (40-60nm), *Gymnema sylvestre* (20-60nm), *Lonicera hypoglauca* (4-25), *Buchanania axillaris* (17–80nm) (Mani et al., 2023; Santhoshkumar et al., 2023; Khateef et al., 2019; Jang et al., 2016).

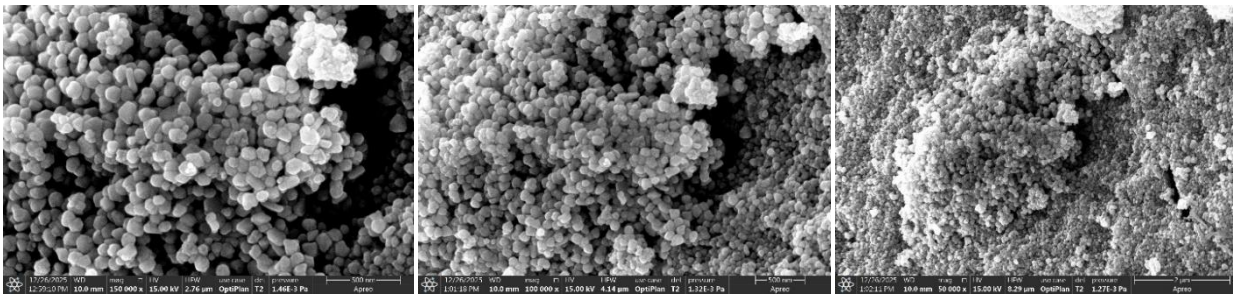

(A) **(B)** **(C)**

Figure 4. SEM micrographs of REA-AgNPs recorded at three different magnifications (scale bars: (A) 100 nm, (B) 200 nm, and (C) 500nm), showing predominantly spherical nanoparticles.

The elemental composition of the nanoparticles was confirmed by EDX analysis (Figure 5A), which exhibited a strong characteristic Ag La peak at ~3 keV, a definitive signature of metallic silver consistent with earlier reports on plant-mediated silver nanoparticle synthesis (Ahmed et al., 2016; Suresh et al., 2014). The absence of significant impurity peaks indicates high purity of the synthesised nanoparticles. Elemental mapping further demonstrated a uniform distribution of silver throughout the analysed area, confirming homogeneous nanoparticle formation (Figure 5B). The combined SEM–EDX results validate the successful green synthesis of silver nanoparticles using *Rubus ellipticus* extract and corroborate the morphological and optical findings obtained from UV–Vis and FTIR analyses.

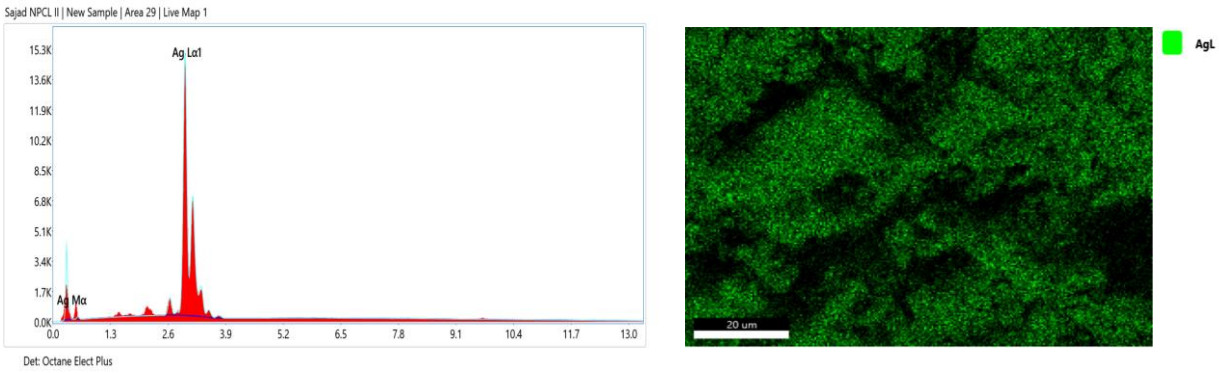

(5A) **(5B)**

Figure 5. **(5A)** EDX spectrum showing a characteristic Ag Lα peak (~3 keV) and **(5B)** Corresponding elemental mapping confirming uniform distribution of silver in the synthesized AgNPs from Rubus ellipticus.

3.4. TEM and SAED Pattern

Transmission electron microscopy (TEM) was employed to determine the size, shape and dispersion of the biosynthesised REAgNPs. TEM micrographs recorded at different magnifications (Figure 6) revealed that the nanoparticles were predominantly spherical in morphology consistent with reports of spherical AgNPs (15-35 nm) from *Diospyros montana* leaf extract (Patra et al., 2021). Particle size distribution of the biosynthesized REAgNPs was analyzed using a histogram constructed from TEM image measurements of 50 individual nanoparticles. As shown in figure 7A, the nanoparticles predominantly fall within the size range of approximately 10–30 nm, with a maximum frequency centered around ~20 nm, matching green-synthesized AgNPs from *Azadirachta indica* (12-28 nm) (Singh et al., 2018). High-resolution TEM images further confirmed the well-defined nanoparticle boundaries, indicating successful formation of discrete silver nanoparticles. The size and morphology observed through TEM corroborate the UV–Vis SPR characteristics and SEM observations, confirming uniform nanoparticle formation through green synthesis.

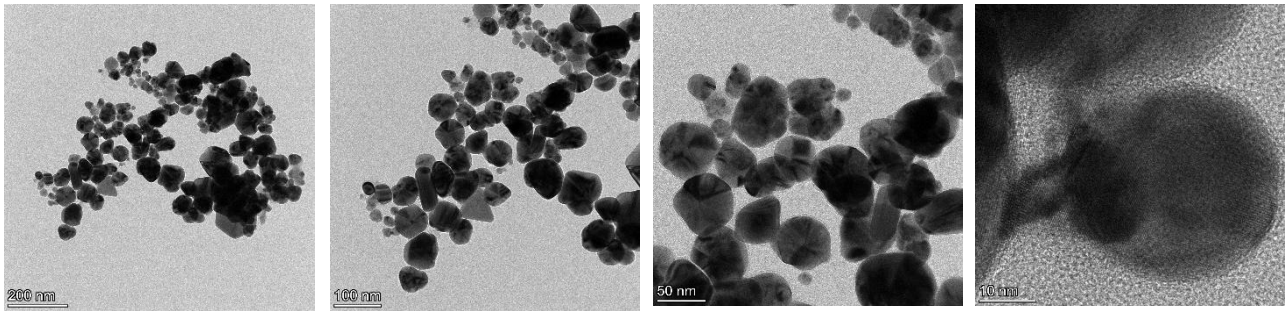

(6A) **(6B)** **(6C)** **(6D)**

Figure 6: TEM micrographs of silver nanoparticles (AgNPs) synthesized using *Rubus ellipticus* extract recorded at different magnifications (Scale bars (A); 200 nm, (B)**;** 100 nm, (C); 50 nm, and (D); 10 nm), revealing predominantly spherical nanoparticles crystalline and polycrystalline nature of the biosynthesized AgNPs.

The crystalline nature of the synthesised nanoparticles was confirmed by Selected Area Electron Diffraction (SAED) analysis (Figure 7B). The SAED pattern exhibited distinct concentric diffraction rings, which are characteristic of crystalline silver and indicate the polycrystalline nature of the REAgNPs. Similar SAED ring patterns confirming polycrystalline AgNPs have been reported in various plant mediated synthesis studies (Keshari et al., 2020; Ajitha et al., 2015). This study confirms the formation of crystalline AgNPs.

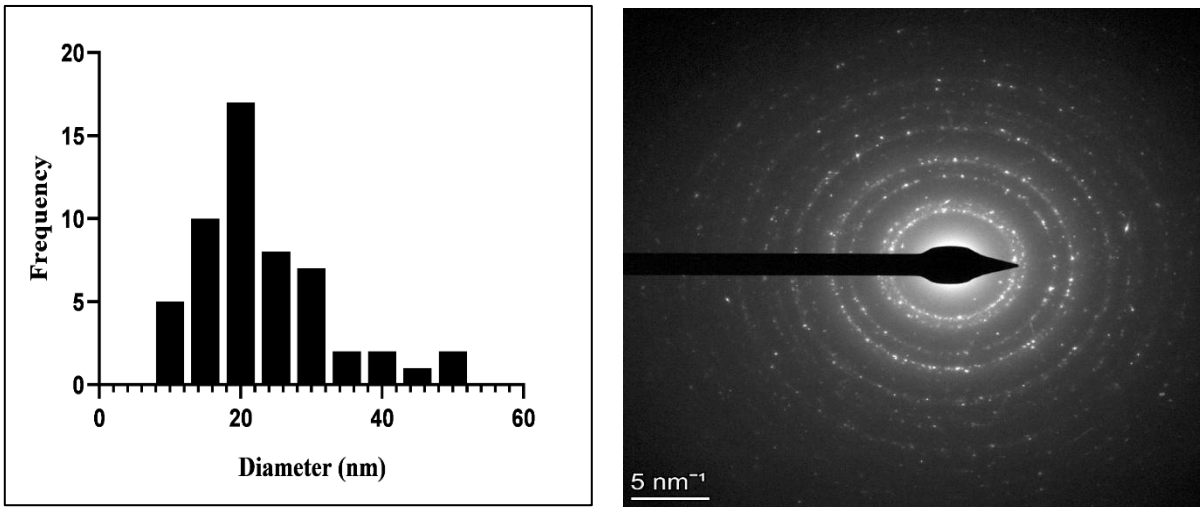

(7A) **(7B)**

Figure 7. **(7A)** Particle size distribution of the biosynthesized REAgNPs. **(7B)** The corresponding SAED pattern shows distinct concentric diffraction rings, confirming the crystalline and polycrystalline nature of the biosynthesized AgNPs.

3.5. AFM Analysis

AFM (2D and 3D) analysis of the REAgNPs showed a heterogeneous, granular surface with nanoscale peaks and valleys across the 1 µm × 1 µm area (Figure 8). The height variation (–18.0 to +17.4 nm) confirmed the presence of uniformly deposited nanoparticles forming moderately aggregated clusters (Figure 8A), aligning well with the 10–30 nm particle size observed in TEM. The smooth contours and merged elevations in the 2D image suggest a phytochemical-derived capping layer from *Rubus ellipticus*, supporting nanoparticle stability (Figure 8B). Comparable AFM roughness patterns have been reported for plant-mediated AgNPs (Bhavi et al., 2024; Kubavat et al., 2022; Singh et al., 2018). Collectively, these findings validate that the REAgNPs are well-capped, uniformly distributed, and morphologically stable, consistent with previously reported green-synthesized AgNPs.

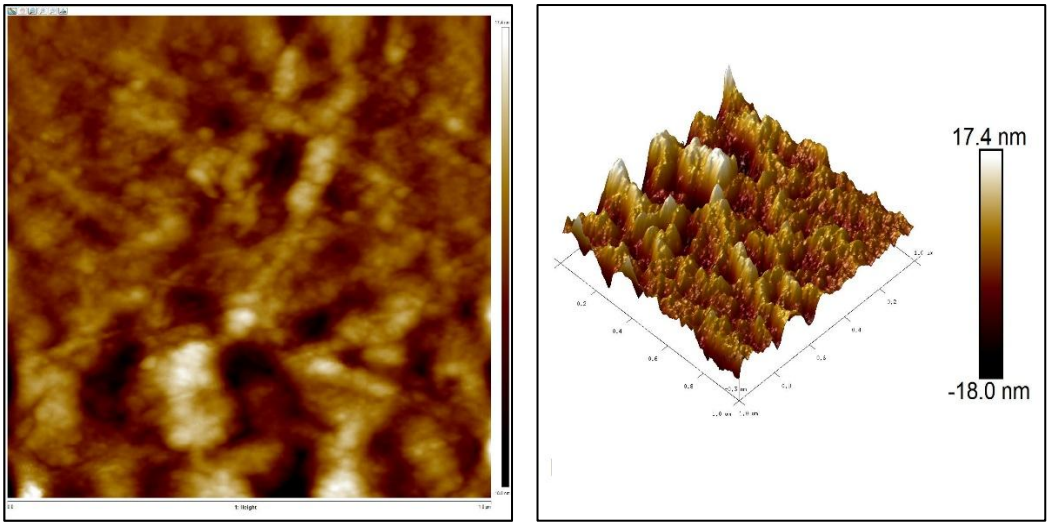

(8A) **(8B)**

Figure 8: AFM 2D (8A) and 3D (8B) images of REAgNPs showing a granular nanoscale surface across the 1 µm × 1 µm scan area. Height variations (–18.0 to +17.4 nm) indicate uniformly deposited, moderately aggregated, phytochemically capped silver nanoparticles.

3.5. XRD Analysis

X-ray diffraction (XRD) analysis was carried out to investigate the crystalline nature and phase composition of the biosynthesised REAgNPs. The XRD pattern (Figure 9) exhibited distinct diffraction peaks at 2θ values corresponding to the crystallographic planes (111), (200), (220) and (311), which are characteristic of the face-centered cubic (fcc) structure of metallic silver and are consistent with standard JCPDS data (04-0783), as reported by Ali et al., 2023. The presence of a strong and sharp (111) diffraction peak indicates a high degree of crystallinity of the synthesised nanoparticles, matching observations in green-synthesized AgNPs from plant

extracts (Thiurunavukkarau et al., 2022; Desalegn et al., 2021; Mehta et al., 2017). No additional peaks corresponding to silver oxide or other impurity phases were detected, confirming the phase purity of the REAgNPs, while minor background features observed in the diffraction pattern may be attributed to residual organic components from plant-derived phytochemicals acting as surface capping agents (Shahzadi et al., 2025). The crystalline nature inferred from the XRD analysis is in good agreement with the concentric diffraction rings observed in the SAED patterns obtained from TEM analysis, further confirming the polycrystalline nature of the biosynthesised silver nanoparticles. Overall, the XRD results validate the successful formation of crystalline, phase-pure silver nanoparticles through green synthesis using *Rubus ellipticus* extract (Makarov et al., 2014).

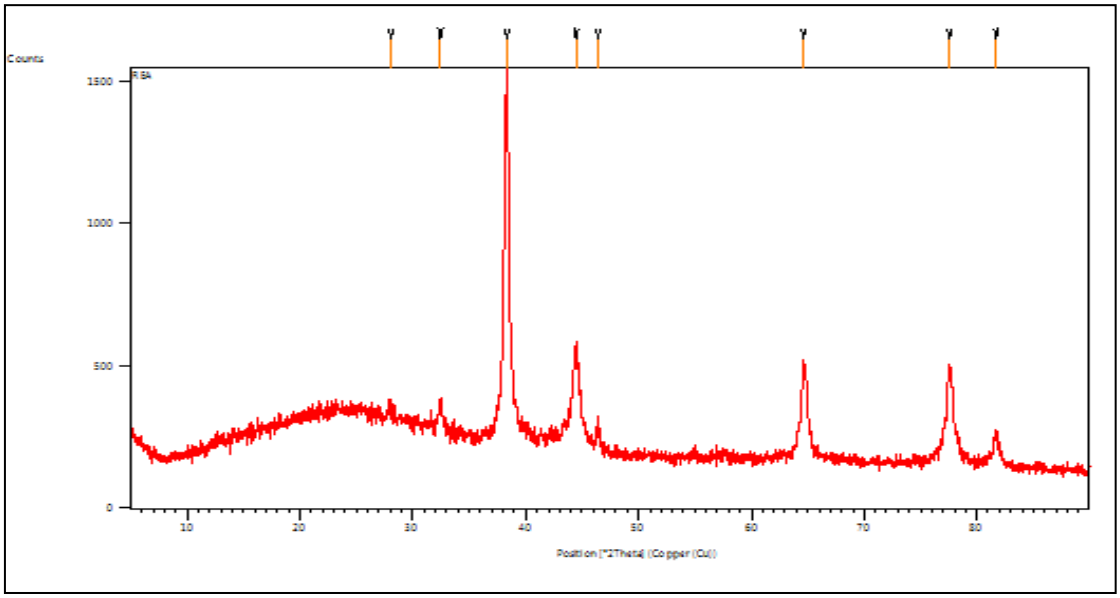

Figure 9. XRD patterns of REA silver nanoparticles. The characteristic diffraction peaks observed at 2θ values around 38°, 44°, 64°, and 77° correspond to the (111), (200), (220), and (311) planes of face-centered cubic (fcc) silver, confirming the successful formation of crystalline Ag nanoparticles.

3.6. Zeta Potential Measurement

Zeta potential analysis was performed to assess the surface charge and colloidal stability of the biosynthesised REAgNPs. The nanoparticles exhibited a negative zeta potential of −22 mV, indicating the presence of surface-bound negatively charged functional groups and suggesting moderate colloidal stability in aqueous suspension (Figure 10), consistent with green-synthesized AgNPs from plant extracts reported by various researchers (Mfon & Amri, 2023; Deepika et al., 2020; Jebril et al., 2020). The relatively narrow distribution profile reflects uniform surface charge

characteristics of the nanoparticles. Negative surface charge in green-synthesised silver nanoparticles is commonly attributed to the adsorption of plant-derived biomolecules such as phenolics, flavonoids and carboxyl-containing compounds, which act as capping agents, generating electrostatic repulsion to reduce aggregation (Chowdhury et al., 2024; Dashora et al., 2022). These negatively charged groups generate electrostatic repulsion between particles, thereby reducing aggregation and enhancing dispersion stability. The observed zeta potential value is consistent with the FTIR results, which confirmed the presence of hydroxyl and carbonyl functional groups on the nanoparticle surface, as similarly noted in *Rubus*-derived AgNPs (Khalil et al., 2023). Thus the zeta potential analysis confirms that the REAgNPs possess sufficient colloidal stability for biological applications, supporting their subsequent use in in vitro anticancer studies.

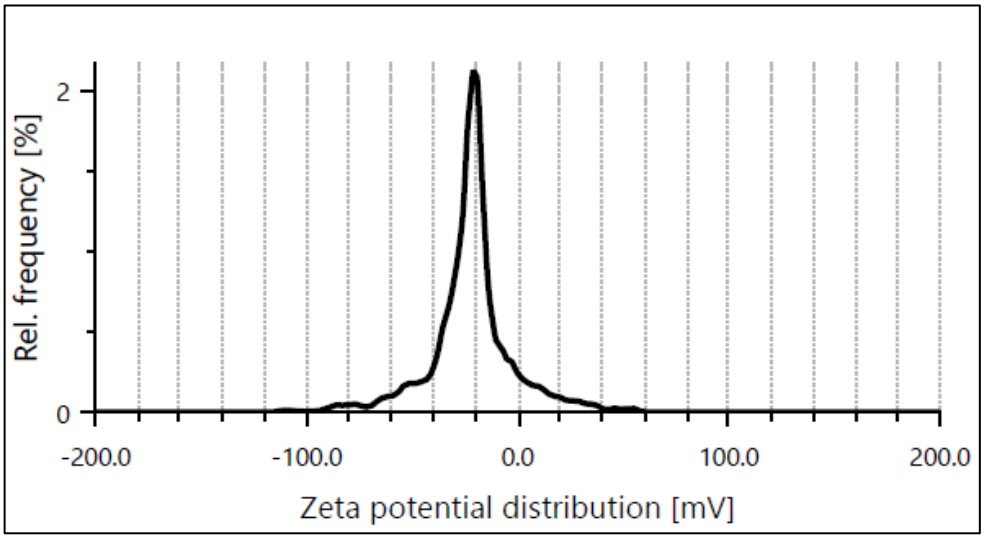

Figure 10. Zeta potential distribution profile of the REAgNPs. (A) The AgNPs show a sharp monodisperse peak at –22.7 mV. The value falls within the typical range for green-synthesized AgNPs (–15 to –35 mV), indicating effective phytochemical capping and good colloidal stability of the nanoparticles.

3.7. Antioxidant Assays

3.7.1. DPPH and H_2O_2 Free Radical Scavenging Assay

The antioxidant potential of REAgNPs was assessed through DPPH and hydrogen peroxide (H_2O_2) scavenging assays, both of which demonstrated a clear concentration-dependent increase in free radical neutralization (Figure 11A and 11B). In the DPPH assay, REAgNPs exhibited strong radical scavenging activity, reflected by a low IC_{50} value, indicating high antioxidant efficiency. At the

highest tested concentration, the scavenging capacity of REAgNPs was comparable to that of the standard antioxidant, ascorbic acid. This potent activity can be attributed to the nanoscale size of the particles, providing a larger reactive surface area, as well as the stabilizing phytochemical corona that enhances electron-donating ability. Similarly, REAgNPs showed effective hydrogen peroxide scavenging, with inhibition increasing progressively with concentration. Their pronounced H_2O_2 neutralizing ability supports the role of silver–phytochemical interactions in facilitating efficient redox reactions. Comparable findings have been reported by Abida et al. (2023) and Khanal et al. (2022), who demonstrated superior DPPH scavenging by plant-derived AgNPs, while Khalil et al. (2023) attributed enhanced H_2O_2 scavenging in *Rubus*-mediated nanoparticles to phytochemical capping that promotes antioxidant activity. Collectively, these results confirm that REAgNPs possess strong free radical scavenging properties, highlighting their ability to mitigate oxidative stress. This significant antioxidant potential of REAgNPs reflects their potential suitability for downstream biological applications, including anticancer investigations.

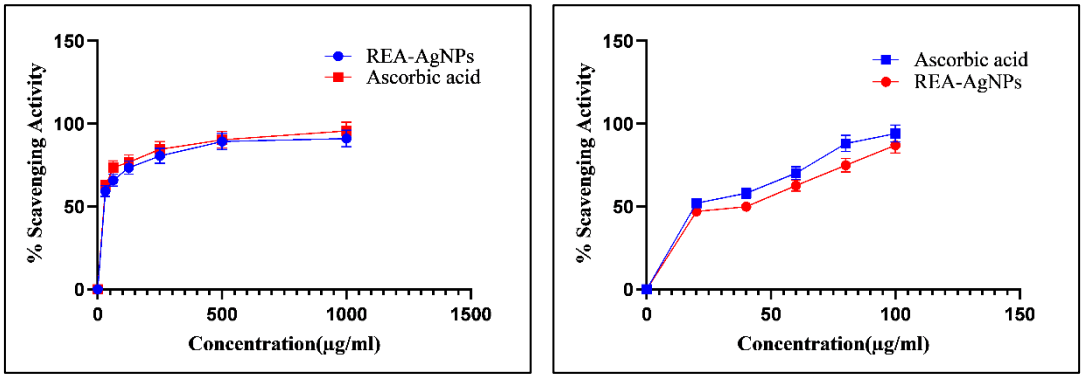

Figure 11. **(A)**: DPPH Free Radical Scavenging activity and (B): Hydrogen Peroxide Scavenging activity of REAgNPs showing a concentration dependent trend, similar to that of the standard, Ascorbic Acid.

3.4. MTT Assay for Cytotoxicity

The antiproliferative activity of REAgNPs against MDA-MB-231 cells was evaluated using the MTT assay. REAgNPs induced a concentration-dependent decrease in cell viability, indicating potent cytotoxic activity (Figure 12). A progressive increase in percentage inhibition was observed with increasing nanoparticle concentration, confirming effective suppression of cancer cell proliferation. A standard chemotherapeutic drug, 5-Fluorouracil (5-FU), was used as a positive control to benchmark the anticancer efficacy of the biosynthesized nanoparticles. The dose–response profile of REAgNPs showed a trend comparable to that of 5-Fluorouracil, particularly at higher concentrations, highlighting their strong antiproliferative potential. Quantitative analysis

revealed that REAgNPs exhibited an IC_{50} value of 30.12 µg/Ml. This IC_{50} value is comparable to, or lower than, those reported for several plant-mediated silver nanoparticles tested against MDA-MB-231 cells, where IC_{50} values typically range between 25–50 µg/mL depending on the plant source and synthesis conditions. Similar concentration-dependent cytotoxic effects have been reported for AgNPs synthesized using medicinal plant extracts rich in phenolics and flavonoids, suggesting that phytochemical-assisted nanoparticle formation plays a critical role in enhancing anticancer activity (Majid, 2025; Zare-Bidaki et al., 2025; Al-Asiri et al., 2024; Gurunathan et ail., 2013;). The observed cytotoxicity of REAgNPs may be attributed to their nanoscale size, high surface area and the presence of surface-bound bioactive phytochemicals, which can facilitate cellular uptake and intracellular interactions (Montazersaheb et al., 2024). Therefore, the MTT assay results demonstrate that REAgNPs exhibit anticancer activity comparable to the standard chemotherapeutic agent 5-Fluorouracil, supporting their potential as eco-friendly nanotherapeutic candidates for the management of triple-negative breast cancer.

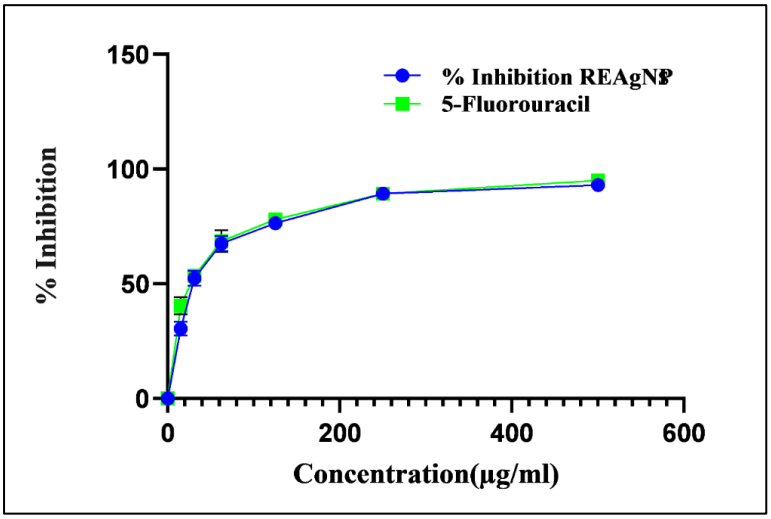

Figure 12. The antiproliferative effect of REAgNPs and the positive control 5-Fluorouracil on MDA-MB-231 cells using the MTT assay showing a concentration dependent trend.

3.5. DAPI Staining

DAPI staining was performed to visualize nuclear morphological alterations associated with apoptosis in MDA-MB-231 cells following treatment with REAgNPs (Figure 13). Untreated control cells exhibited uniformly stained, intact nuclei with regular morphology, indicating normal chromatin organization and cell viability (13A). In contrast, cells treated with REAgNPs at their IC_{50} concentration displayed pronounced nuclear abnormalities characteristic of apoptosis (13B). These included chromatin condensation, nuclear fragmentation, cell shrinkage and formation of apoptotic bodies, as evidenced by intensely stained and irregularly shaped nuclei. The reduction

in nuclear number and the presence of fragmented chromatin further indicate loss of cell viability following REAgNP exposure. Such nuclear alterations are hallmark features of apoptosis and are commonly reported in cancer cells treated with green-synthesised silver nanoparticles. Similar DAPI staining patterns, reflecting apoptotic nuclear damage, have been observed in MDA-MB-231 cells exposed to plant-mediated AgNPs, supporting the involvement of programmed cell death rather than necrotic damage (Alhajri et al., 2021; Bin-Jumah et al., 2020). The observed nuclear disintegration in the present study is consistent with the antiproliferative effects detected in the MTT assay and suggests that REAgNP-induced cytotoxicity is mediated through apoptosis. Therefore, DAPI staining confirms that REAgNPs effectively induce apoptotic nuclear changes in MDA-MB-231 cells, providing morphological evidence for apoptosis.

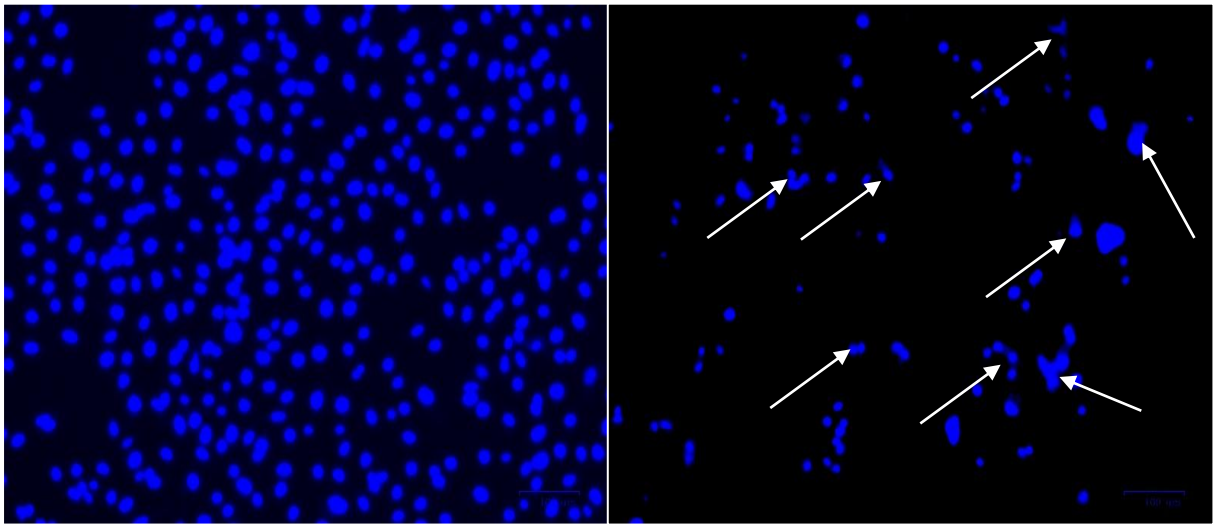

(13A) **(13B)**

Figure 13. Images **(13A)** Untreated MDA-MB-231 cells; **(13B)** Treated MDA-MB-231 cells with RE-AgNPs (IC_{50}:30.12µL/mL); White arrows: Membrane Blebbing, Cell Shrinkage, Chromatin Condensation, Nuclear Fragmentation and Aggregation of Apoptotic Bodies; Imaging by Fluorescence Microscope (Nikon Eclipse Ts2, Japan) at 40x magnification.

3.6.Rhodamine Staining for Detection of Mitochondrial Dysfunction

Mitochondrial membrane potential (MMP) disruption, a key early event in intrinsic apoptosis, was evaluated in MDA-MB-231 cells using Rhodamine-123 staining following treatment with REAgNPs (Figure 14). Untreated control cells exhibited intense green fluorescence, indicating intact mitochondrial membrane potential and healthy mitochondrial function (14A). In contrast, cells treated with REAgNPs at their IC_{50} concentration showed a marked reduction in Rhodamine-

123 fluorescence intensity, reflecting significant loss of mitochondrial membrane potential (14B). Quantitative analysis further confirmed a substantial decrease in mean fluorescence intensity in treated cells compared to controls, indicating mitochondrial depolarization (14C). The diminished fluorescence suggests impaired mitochondrial integrity, which is a hallmark of apoptosis mediated via the intrinsic pathway. Loss of MMP is known to facilitate the release of pro-apoptotic factors from mitochondria, such as cytochrome c, leading to downstream activation of caspase cascades (Raja et al., 2020). Similar reductions in Rhodamine-123 fluorescence and MMP collapse have been reported in breast cancer and other cancer cell lines treated with green-synthesized silver nanoparticles, highlighting mitochondrial dysfunction as a central mechanism of AgNP-induced apoptosis (Pandey et al., 2025; Wani et al., 2023; Faheem et al., 2022). The observed MMP disruption in the present study correlates well with the cytotoxic effects observed in the MTT assay and the nuclear alterations detected by DAPI staining. Therefore, Rhodamine-123 staining confirms that REAgNPs induce apoptosis in MDA-MB-231 cells through mitochondrial membrane depolarization, providing strong evidence for the involvement of the intrinsic apoptotic pathway.

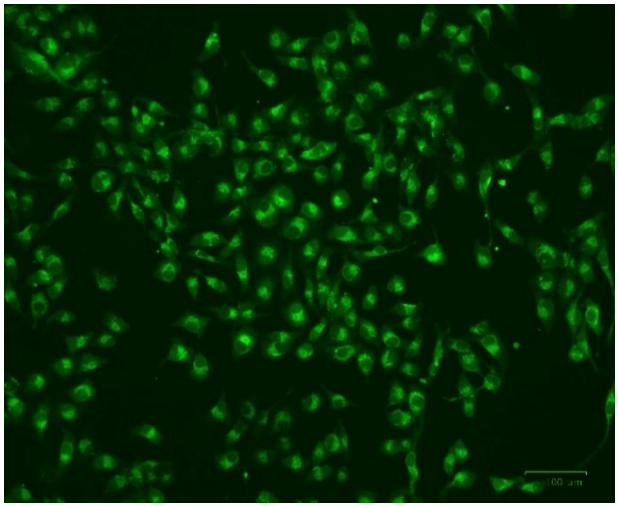

(14A)

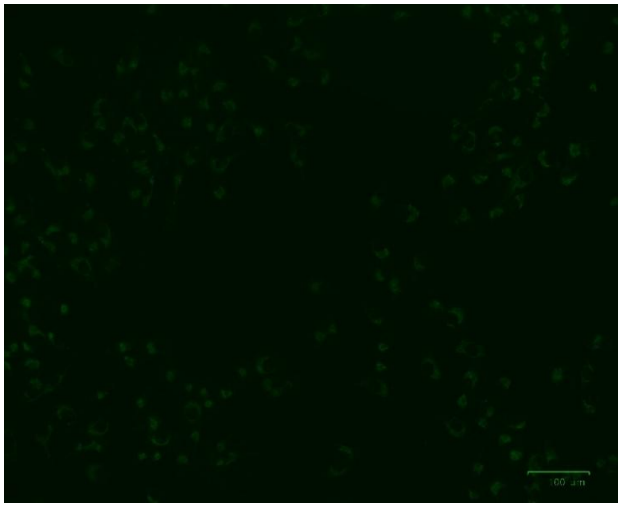

(14B)

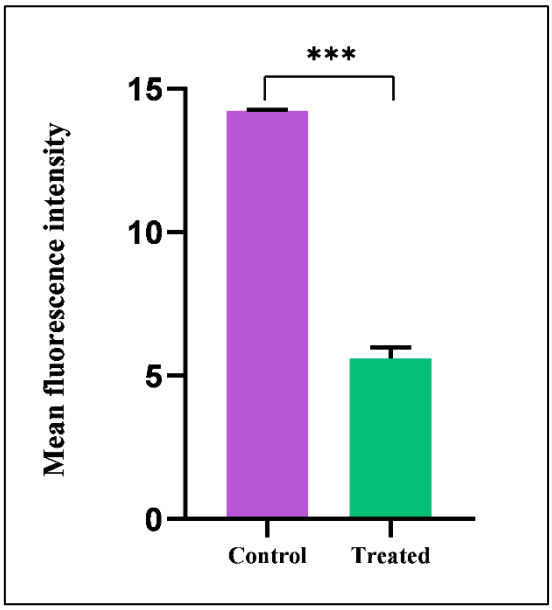

(14C)

Figure 14. Images (**14A**) depict Untreated cells; **(14B)**: Treated cells with REAgNPs (IC_{50}=30.12µL/mL) **(14C)** Representative histogram showing fluorescence changes in MDA-MB-231 cells. Green signal cells were quantified using Image-J software. Data Values are mean ± SD of triplicated experiment; ANOVA/GraphPad Prism (8); Asterisk (*), (**) and (***) indicates $p \leq 0.05$, $p \leq 0.01$ and $p \leq 0.001$; Imaging by Fluorescence Microscope (Nikon Eclipse Ts2, Japan) at 40x magnification.

3.7.DNA Fragmentation Assay

DNA fragmentation analysis was performed to further confirm apoptosis induction in MDA-MB-231 cells following treatment with REAgNPs (Figure 15). Agarose gel electrophoresis of genomic DNA isolated from untreated control cells showed intact, high–molecular weight DNA with no

evidence of fragmentation, indicating normal cellular integrity. In contrast, cells treated with REAgNPs at their IC_{50} concentration (30.12 µg/mL) for 24 h exhibited pronounced DNA fragmentation, as evidenced by the presence of smeared and fragmented DNA bands. This pattern is characteristic of apoptotic DNA cleavage resulting from endonuclease activation during programmed cell death. The appearance of fragmented DNA in REAgNP-treated cells confirms irreversible nuclear damage and supports apoptosis as the primary mode of cell death. DNA fragmentation is a late-stage hallmark of apoptosis and typically follows mitochondrial dysfunction and caspase activation (Cao et al., 2022; Kari et al., 2022; Majtnerová & Roušar, 2018). The observed DNA damage in the present study is consistent with the loss of mitochondrial membrane potential detected by Rhodamine-123 staining and the nuclear condensation and fragmentation observed in DAPI-stained cells. Similar apoptotic DNA fragmentation patterns have been widely reported in cancer cells treated with green-synthesised silver nanoparticles, further validating the apoptotic mechanism (Irani et al., 2025; Pushparaj et al., 2023; Habeeb et al., 2022).

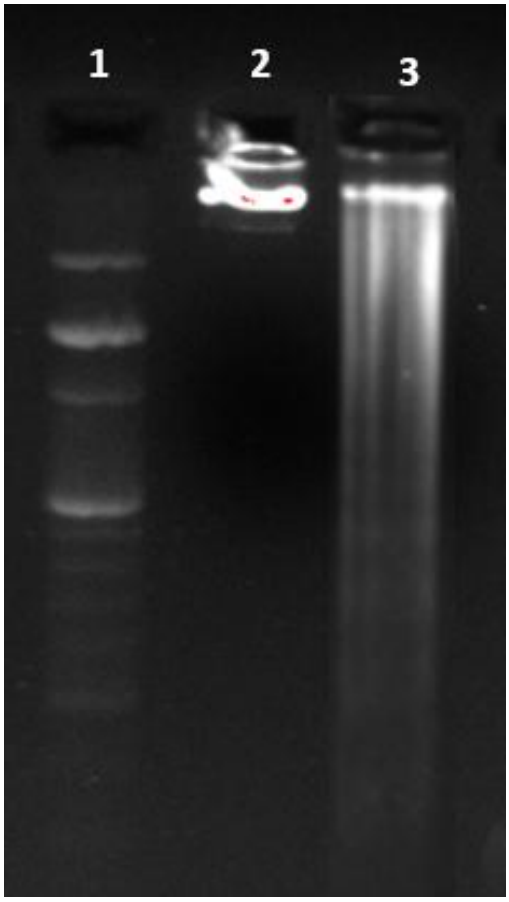

Figure 15. This figure shows the DNA fragmentation assay confirming apoptosis. Lane 1: 100 bp DNA ladder; Control lane (2) displays intact DNA, while REAgNP-treated cells (lane 3) at IC_{50} concentrations show clear DNA fragmentation after 24 hours. The smeared pattern indicates apoptotic DNA damage compared to untreated controls.

3.12. Annexin V–FITC/PI Apoptosis Assay

Apoptosis induction by REAgNPs in MDA-MB-231 cells was quantitatively assessed using Annexin V-FITC/PI dual staining followed by flow cytometry (Figure 16). In untreated control cells, the majority of the population remained viable, with 85.8% live cells (Annexin V^-/PI^-), while only 1.0% early apoptotic (Annexin V^+/PI^-), 10.5% late apoptotic (Annexin V^+/PI^+) and 2.6% necrotic (Annexin V^-/PI^+) cells were observed, indicating minimal basal apoptosis (16A and 16C). In contrast, REAgNP-treated cells (30.12 µg/mL, 24 h) exhibited a pronounced shift toward apoptotic populations. The percentage of live cells decreased markedly to 20.6%, accompanied by a significant increase in early apoptotic cells (13.6%) and a dominant late apoptotic population (65.7%), while necrotic cells remained minimal (0.1%) (16B and 16C). This substantial rise in Annexin V–positive cells confirms effective apoptosis induction following REAgNP treatment. The predominance of late apoptotic cells indicates progression of apoptosis rather than acute membrane damage, suggesting that REAgNP-mediated cytotoxicity occurs primarily through programmed cell death rather than necrosis. Externalization of phosphatidylserine, reflected by increased Annexin V positivity, represents a key early event in apoptosis and aligns with mitochondrial membrane potential loss and nuclear fragmentation observed in previous assays. These findings are consistent with reports other researchers (Hosseini et al., 2024; Yesilot et al., 2023;Joseph et al., 2021). Therefore, Annexin V/PI analysis provides strong quantitative evidence that REAgNPs effectively trigger apoptosis in MDA-MB-231 cells.

Control **Treatment**

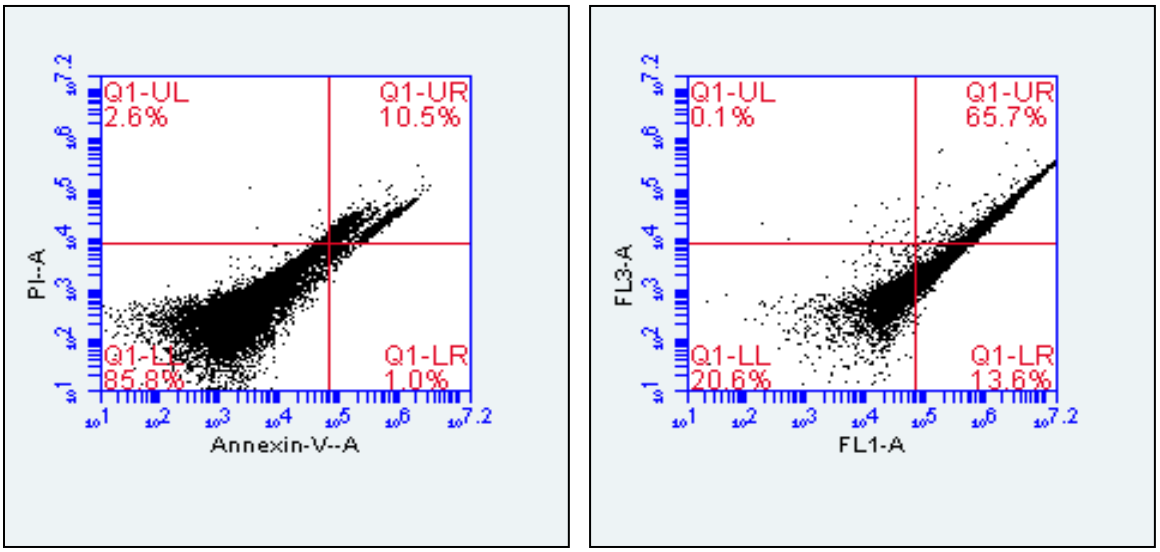

(16A) **(16B)**

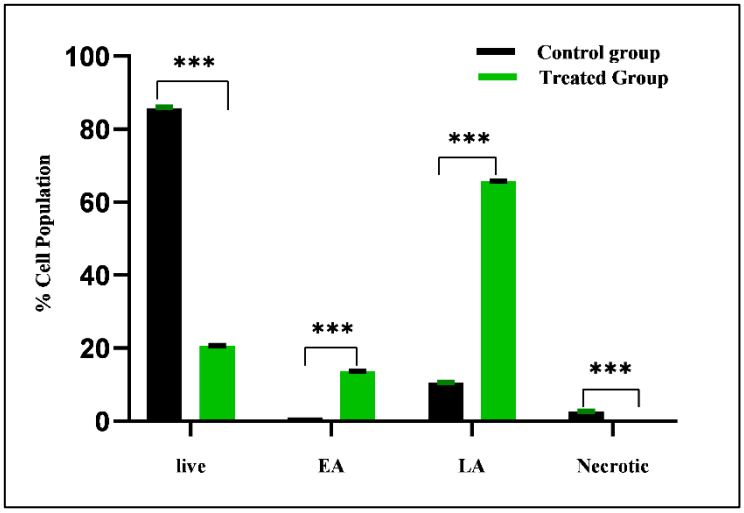

(16C)

Figure 16. (16A): Control: Untreated cells; **(16B)** Treated cells with REAgNPs (30.12µL/mL for 24h; Flow cytometry analysis shows total percentages of cells from four different quadrants (Q1 =Live cells, Q2 = Early apoptosis (EA), Q3 =Late apoptosis, Q4=Necrosis). **(16C)** Bar graph represents values of cell percentages. Data Values are mean ± SD of triplicated experiment; One Way ANOVA/GraphPad Prism (8) ; Asterisk (*), (**) and (***) indicates significance $p \leq 0.05$, $p \leq 0.01$ and $p \leq 0.001$ compared to control group

3.8.Cell Cycle Analysis

Cell cycle distribution of MDA-MB-231 cells following treatment with REAgNPs was analyzed by flow cytometry to determine whether growth inhibition was associated with cell cycle arrest (Figure 17). Untreated control cells displayed a typical proliferative profile, with 32.0% of cells in G0/G1 phase, 56.7% in S phase and 14.4% in G2/M phase, indicating active DNA synthesis and cell division (17A and 17C). In contrast, REAgNP-treated cells (30.12 µg/mL, 24 h) exhibited a pronounced alteration in cell cycle progression. A substantial accumulation of cells was observed in the G0/G1 phase (66.4%), accompanied by a marked reduction in the S phase population (29.8%) and a decrease in G2/M phase cells (5.8%) (17B and 17C). This shift indicates effective G0/G1 phase arrest, suggesting inhibition of DNA synthesis and suppression of cell cycle progression. G0/G1 arrest is a well-recognized mechanism associated with apoptosis induction and is often linked to mitochondrial dysfunction and activation of downstream apoptotic pathways. The observed cell cycle blockade in the present study is consistent with the loss of mitochondrial membrane potential, nuclear fragmentation, DNA damage and Annexin V-positive apoptotic populations detected in earlier assays. Similar G0/G1 arrest patterns have been reported by various researchers, supporting the role of AgNPs in disrupting cell cycle regulatory checkpoints (Liu et al., 2025; Takáč et al., 2023; Mishra et al., 2021; Vallinayagam et al., 2021). Hence, the cell cycle analysis confirms that REAgNPs inhibit proliferation of MDA-MB-231 cells by inducing G0/G1 phase arrest, thereby contributing to apoptosis-mediated growth suppression.

Control **Treatment**

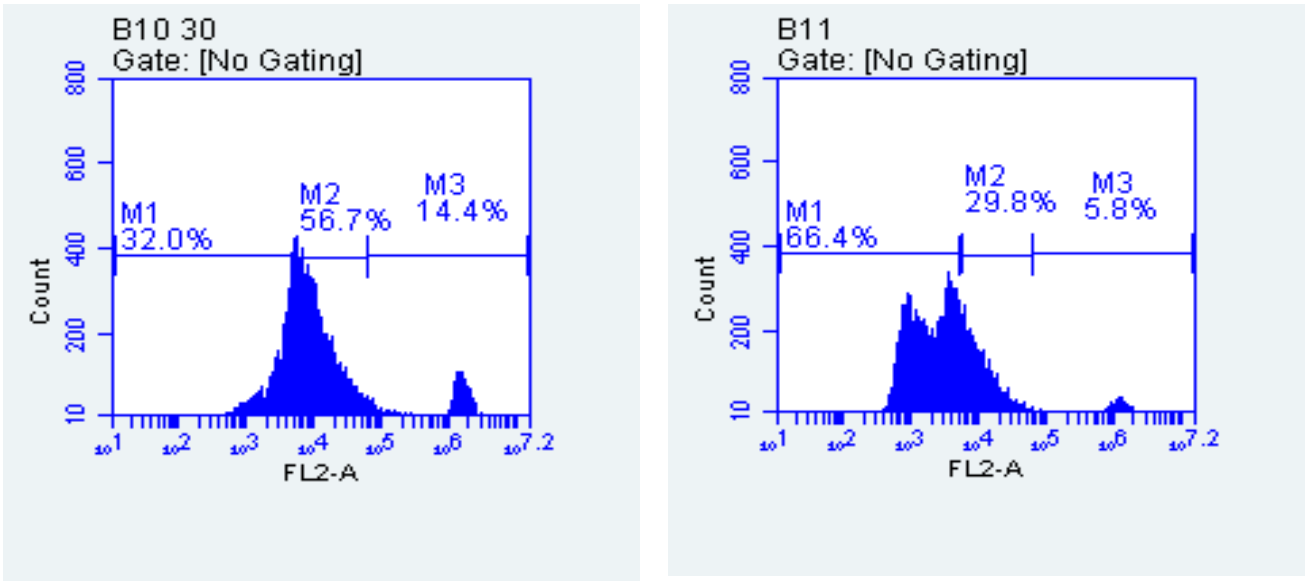

(17A) **(17B)**

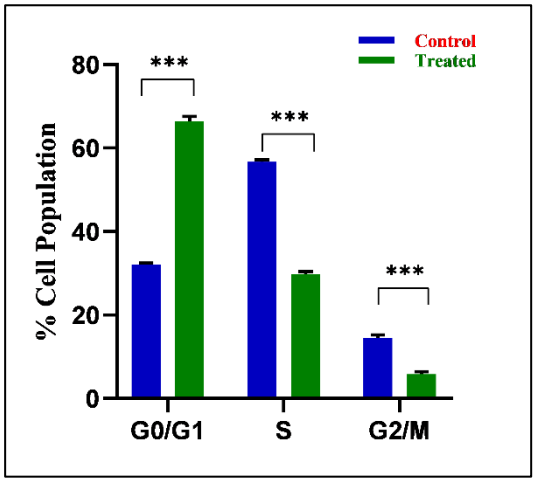

(17C)

Figure 17. (17A): Control: untreated cells; **(17B)** Treated cells with REAgNPs (30.12µL) for 24h; Flow cytometry analysis shows percentages of cells according to the DNA content in each cell cycle phases, **(17C)** Bar graph represents values of cell percentages in the G0/G1(2N), S(2N-4N) ,G2/M(4N) phase. Data Values are mean ± SD of triplicated experiment; One Way ANOVA/GraphPad Prism (8); Asterisk (*), (**) and (***) indicates significance $p \leq 0.05$, $p \leq 0.01$, $p \leq 0.001$ and ns; not significant compared to control group.

3.9.Western Blot Analysis of Caspase-3

Western blot analysis was performed to evaluate the activation of caspase-3, a key executioner protease in apoptosis, in MDA-MB-231 cells treated with REAgNPs (Figure 18). Untreated control cells exhibited minimal expression of cleaved caspase-3, indicating low basal apoptotic activity under normal culture conditions (18A and 18B). In contrast, cells treated with REAgNPs at their IC_{50} concentration (30.12 µg/mL) for 24 h showed a marked increase (~ 2 fold) in the expression of cleaved caspase-3 (~17 kDa) compared to control cells (18A and 18B). The enhanced band intensity in treated samples clearly indicates activation of caspase-3 following REAgNP exposure. β-actin (~42 kDa) expression remained consistent across all samples, confirming equal protein loading and validating the observed changes in caspase-3 expression. Activation of Caspase-3 represents a critical downstream event in the apoptotic cascade and signifies irreversible commitment to programmed cell death (Asadi et al., 2022). The observed increase in cleaved caspase-3 expression is consistent with mitochondrial membrane potential loss, DNA fragmentation, nuclear condensation and Annexin V–positive apoptotic populations detected in earlier assays. Similar activation of caspase-3 has been widely reported in breast cancer cells treated with green-synthesised silver nanoparticles, supporting the involvement of the intrinsic (mitochondria-mediated) apoptotic pathway (Montazersaheb et al., 2024; Kim et al., 2018; Plackal et al., 2018). Overall, the Western blot results provide strong molecular evidence that REAgNPs induce apoptosis in MDA-MB-231 cells through activation of caspase-3, thereby confirming execution-phase apoptosis and conclusively supporting the proposed anticancer mechanism.

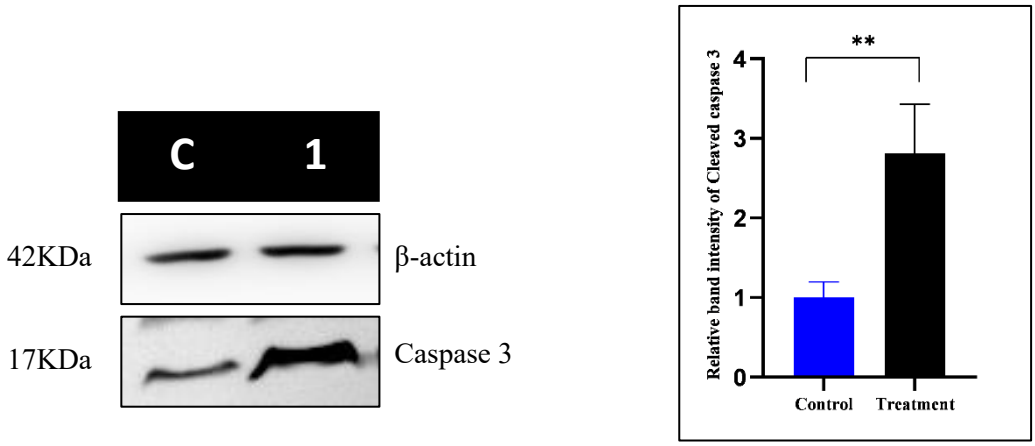

(18A) **(18B)**

Figure 17. (18A): Western blot analysis of cleaved caspase-3 expression in control and REAgNP-treated cells. Proteins (approximately 50µg) were resolved on 12% SDS-PAGE followed by western blot analysis using an Anti-cleaved caspase-3 (Asp175) antibody against cleaved caspase-3. Lane C represents untreated control cells, while lane 1 represents cells treated with REAgNPs at the IC_{50} concentration for 24 h. Increased band intensity in treated cells indicates activation of cleaved caspase-3. β-actin was used as the loading control, indicating the same amount of proteins applied. **(17B)**: Histogram representing fold changes in the activation of the apoptosis executioner protein Caspase3

4. Conclusion

In the present study, silver nanoparticles were successfully phytofabricated using *Rubus ellipticus* aqueous extract through an eco-friendly and sustainable green synthesis approach. Comprehensive physicochemical characterization confirmed the formation of stable, spherical, crystalline REAgNPs, effectively capped by plant-derived biomolecules. The biosynthesised nanoparticles exhibited enhanced antioxidant activity compared to the crude extract, indicating improved free radical scavenging potential following nanoparticle formulation. Importantly, REAgNPs demonstrated significant antiproliferative activity against triple-negative breast cancer MDA-MB-231 cells in a concentration-dependent manner. Mechanistic investigations revealed that REAgNP-induced cytotoxicity was mediated through mitochondrial dysfunction, DNA damage, cell-cycle arrest at the G0/G1 phase and activation of the intrinsic apoptotic pathway, as evidenced by nuclear fragmentation, phosphatidylserine externalization and caspase-3 activation. Hence, this study highlights *Rubus ellipticus*-derived silver nanoparticles as promising eco-friendly nanotherapeutic candidates for triple-negative breast cancer management. Further in vivo investigations and toxicity assessments are warranted to validate their therapeutic applicability and clinical potential.

Acknowledgement: We express our sincere gratitude to Dr. Shreekar Pant from the Centre for Biodiversity Studies, BGSBU, Rajouri, J&K, for his valuable assistance in plant identification. We also acknowledge the laboratory facilities provided by GNDU, Amritsar and BGSBU, Rajouri. We extend our heartfelt thanks to Dr. Shoeb Ahmad, Dr. Tanvir ul Hassan Dar and Dr. Arif Tasleem Jan for kindly allowing us to use their laboratory facilities and for their continuous support throughout the study. Furthermore, we are thankful to the University Grants Commission (UGC) and the Indian Council of Medical Research, Government of India (ICMR, GOI) for providing essential funding assistance.

Conflict of Interest

The authors confirm that they have no conflicts of interest or personal relationships that could have influenced the work reported in this paper.

Credit author statement

Darakhshan Javaid: Writing and Figures, Experimentation, Formal Analysis, Final Draft preparation. **Shahid Yousuf Ganie**: Writing and Figures, experimentation, Formal analysis. **Sheikh Showkat Ahmad**: Experimentation, Proof reading. **Satwinderjeet Kaur**: Formal analysis, Proofreading. **Mohd. Salim Reshi***: Conceptualization, Supervision, Project Administration, Resources, Writing – review, editing and Final Draft Preparation.

Data availability statement

The data generated in the present study may be requested from the corresponding author.

Declaration of AI Tool Usage

During the preparation of this work, the authors used ChatGPT, an AI-based language assistance tool, to improve the clarity and readability of the manuscript. After using this tool, the authors thoroughly reviewed and edited the content and take full responsibility for the final version of the article.

Ethics declaration: not applicable.

References

1. Wilkinson, L., & Gathani, T. (2022). Understanding breast cancer as a global health concern. *The British journal of radiology*, *95*(1130), 20211033.
2. Javaid, D., Ganie, S. Y., Qadri, S. S., Reyaz, A., & Reshi, M. S. (2025). Eco-friendly nanotherapeutics: Metallic nanoparticles for targeting breast cancer. *European Journal of Pharmacology*, 177603.
3. Cai, S. L., Liu, J. J., Liu, Y. X., Yu, S. H., Liu, X., Lin, X. Q., ... & Zhang, J. (2023). Characteristics of recurrence, predictors for relapse and prognosis of rapid relapse triple-negative breast cancer. *Frontiers in Oncology*, *13*, 1119611.
4. Chaturvedi, V. K., Singh, A., Singh, V. K., & Singh, M. P. (2019). Cancer nanotechnology: a new revolution for cancer diagnosis and therapy. *Current drug metabolism*, *20*(6), 416-429.
5. Reshi, M. S. (2018, January). Amelioration against paracetomol induced oxidative DNA damage by the therapy of gold nanoparticles in rats. In *Proceedings of the international conference on emerging researches in bioscience: souvenir and abstract* (pp. 36-36).
6. Dhir, R., Chauhan, S., Subham, P., Kumar, S., Sharma, P., Shidiki, A., & Kumar, G. (2024). Plant-mediated synthesis of silver nanoparticles: unlocking their pharmacological potential–a comprehensive review. *Frontiers in Bioengineering and Biotechnology*, *11*, 1324805.
7. Reshi, M. S., Bhatia, G., Yadav, D., Uthra, C., Arora, S. S. J. S., & Shukla, S. (2016). Pure silver nanoparticles showed potential anticancer effect on colon and breast cancer cell lines. *Octa Journal of Biosciences*, *4*(2).
8. Shrivastava, S., Nirala, S. K., Reshi, M. S., Shukla, S., Sharma, A., & Uthra, C. (2019). Protective efficacy of vitamin F against acrylamide induced toxicity: studies on oxidative stress biomarkers. *The Open Biomarkers Journal*, *9*(1).
9. Sheikh, T. A., Ganie, S. Y., Javaid, D., Yadav, D., & Reshi, M. S. (2024). Apium leptophyllum: Phytochemical analysis and cytotoxicity evaluation. *Pharmacological Research-Natural Products*, *4*, 100075.
10. Reyaz, A., Javaid, D., Qadri, S. S., Ganie, S. Y., & Reshi, M. S. (2025). Bisphenol A and reproductive health: a comprehensive overview of toxicological effect. *Toxicological Research*, *41*(6), 553-567.
11. Wu, H., Lin, J., Liu, P., Huang, Z., Zhao, P., Jin, H., ... & Gu, N. (2016). Reactive oxygen species acts as executor in radiation enhancement and autophagy inducing by AgNPs. *Biomaterials*, *101*, 1-9.
12. Nguyen, N. P. U., Dang, N. T., Doan, L., & Nguyen, T. T. H. (2023). Synthesis of silver nanoparticles: from conventional to 'modern'methods—a review. *Processes*, *11*(9), 2617.
13. Kirubakaran, D., Wahid, J. B. A., Karmegam, N., Jeevika, R., Sellapillai, L., Rajkumar, M., & SenthilKumar, K. J. (2026). A comprehensive review on the green synthesis of nanoparticles: advancements in biomedical and environmental applications. *Biomedical Materials & Devices*, *4*(1), 388-413.
14. Chowdhury, S. S., Ibnat, N., Hasan, M., & Ghosh, A. (2024). Medicinal Plant-Based nanoparticle synthesis and their diverse applications. In *Ethnopharmacology and OMICS Advances in Medicinal Plants Volume 2: Revealing the Secrets of Medicinal Plants* (pp. 213-250). Singapore: Springer Nature Singapore.

15. Pattabhiramaiah, M., Rajarathinam, B., & Shanthala, M. (2020). Nanoparticles and their application in folklore medicine as promising biotherapeutics. *Functional bionanomaterials: From biomolecules to nanoparticles*, 73-110.
16. Sastry, K. S., Mandal, B., Hammond, J., Scott, S. W., & Briddon, R. W. (2020). *Rubus ellipticus* (Yellow Himalayan raspberry). In *Encyclopedia of Plant Viruses and Viroids* (pp. 2109-2109). New Delhi: Springer India.
17. Lee, B. J., Kanaan, M. H. G., Abdullah, S. S., & Ghasemian, A. (2025). Plant-Derived Nanoparticles in Cancer Therapy: A Comprehensive Review of Recent Advances and Future Prospects. *OBM Genetics*, *9*(3), 1-22.
18. Bindhu, M. R., & Umadevi, M. (2015). Antibacterial and catalytic activities of green synthesized silver nanoparticles. *Spectrochimica acta part A: molecular and biomolecular spectroscopy*, *135*, 373-378.
19. Jadid, N., Hidayati, D., Hartanti, S. R., Arraniry, B. A., Rachman, R. Y., & Wikanta, W. (2017, June). Antioxidant activities of different solvent extracts of Piper retrofractum Vahl. using DPPH assay. In *AIP conference proceedings* (Vol. 1854, No. 1, p. 020019). AIP Publishing LLC.
20. Ruch, R. J., Cheng, S. J., & Klaunig, J. E. (1989). Prevention of cytotoxicity and inhibition of intercellular communication by antioxidant catechins isolated from Chinese green tea. *Carcinogenesis*, *10*(6), 1003-1008.
21. Siddiqui, M. A., Siddiqui, H. H., Mishra, A., & Usmani, A. (2020). Evaluation of cytotoxic activity of Lavandula stoechas aerial parts fractions against HepG2 cell lines. *Current Bioactive Compounds*, *16*(9), 1281-1289.J. J. Lemasters and A. L. Nieminen, "Mitochondrial oxygen radical formation during reductive and oxidative stress to intact hepatocytes," *Bioscience Reports* 17 (1997): 281–291.
22. Shashi, J. Singh, R. J. Madhusudana, S. A. Kumar and Q. G. Nabi, "A novel lignan composition from *Cedrus deodara* induces apoptosis and early nitric oxide generation in human leukemia Molt-4 and HL-60 cells," *Nitric Oxide* 14(1) (2006): 72–88.
23. Krishan, "Rapid flow cytofluorometric analysis of mammalian cell cycle by propidium iodide staining," *Journal of Cell Biology* 66 (1975): 188–193.
24. H. Chehade, A. Fox, G. G. Mor and A. B. Alvero, "Determination of caspase activation by western blot," *Detection of Cell Death Mechanisms: Methods and Protocols* (2021)1–12.
25. Khurana, K., & Jaggi, N. (2021). Localized surface plasmonic properties of Au and Ag nanoparticles for sensors: a review. *Plasmonics*, *16*(4), 981-999.
26. Khanal, L. N., Sharma, K. R., Paudyal, H., Parajuli, K., Dahal, B., Ganga, G. C., ... & Kalauni, S. K. (2022). Green synthesis of silver nanoparticles from root extracts of *Rubus ellipticus* Sm. and comparison of antioxidant and antibacterial activity. *Journal of Nanomaterials*, *2022*(1), 1832587.
27. Habeeb Rahuman, H. B., Dhandapani, R., Narayanan, S., Palanivel, V., Paramasivam, R., Subbarayalu, R., ... & Muthupandian, S. (2022). Medicinal plants mediated the green synthesis of silver nanoparticles and their biomedical applications. *IET nanobiotechnology*, *16*(4), 115-144.
28. AlQahtani, F. S., AlShebly, M. M., Govindarajan, M., Senthilmurugan, S., Vijayan, P., & Benelli, G. (2017). Green and facile biosynthesis of silver nanocomposites using the aqueous extract of *Rubus ellipticus* leaves: toxicity and oviposition

deterrent activity against Zika virus, malaria and filariasis mosquito vectors. *Journal of Asia-Pacific Entomology*, *20*(1), 157-164.

29. Mani, S. T., Jayakumar, P., Pavithra, M. E., Saranya, K., Rathinavel, T., & Ammashi, S. (2023). Green Synthesis and Characterization of Silver Nanoparticles from Eclipta alba and Its Activity Against Triple-Negative Breast Cancer Cell Line (MDA-MB-231). *Molecular Biotechnology*, 1-11.
30. Santhoshkumar, M., Perumal, D., Narenkumar, J., Ramachandran, V., Muthusamy, K., Alfarhan, A., & David, E. (2023). Potential use of bio functionalized nanoparticles to attenuate triple negative breast cancer (MDA-MB-231 cells). *Bioprocess and biosystems engineering*, *46*(6), 803-811.
31. Jang, S. J., Yang, I. J., Tettey, C. O., Kim, K. M., & Shin, H. M. (2016). In-vitro anticancer activity of green synthesized silver nanoparticles on MCF-7 human breast cancer cells. *Materials Science and Engineering: C*, *68*, 430-435.
32. Khateef, R., Khadri, H., Almatroudi, A., Alsuhaibani, S. A., Mobeen, S. A., & Khan, R. A. (2019). Potential in-vitro anti-breast cancer activity of green-synthesized silver nanoparticles preparation against human MCF-7 cell-lines. *Advances in Natural Sciences: Nanoscience and Nanotechnology*, *10*(4), 045012.
33. Suresh, G., Gunasekar, P. H., Kokila, D., Prabhu, D., Dinesh, D., Ravichandran, N., ... & Siva, G. V. (2014). Green synthesis of silver nanoparticles using Delphinium denudatum root extract exhibits antibacterial and mosquito larvicidal activities. Spectrochimica Acta Part A: Molecular and Biomolecular Spectroscopy, 127, 61-66.
34. Ahmed, S., Ahmad, M., Swami, B. L., & Ikram, S. (2016). A review on plants extract mediated synthesis of silver nanoparticles for antimicrobial applications: a green expertise. Journal of advanced research, 7(1), 17-28.
35. Keshari, A. K., Srivastava, R., Singh, P., Yadav, V. B., & Nath, G. (2020). Antioxidant and antibacterial activity of silver nanoparticles synthesized by Cestrum nocturnum. *Journal of Ayurveda and integrative medicine*, *11*(1), 37-44.
36. Ajitha, B., Reddy, Y. A. K., & Reddy, P. S. (2015). Green synthesis and characterization of silver nanoparticles using Lantana camara leaf extract. *Materials science and engineering: C*, *49*, 373-381.
37. Kubavat, K., Trivedi, P., Ansari, H., Kongor, A., Panchal, M., Jain, V., & Sindhav, G. (2022). Green synthesis of silver nanoparticles using dietary antioxidant rutin

and its biological contour. *Beni-Suef University Journal of Basic and Applied Sciences*, *11*(1), 115.

38. Singh, T., Jyoti, K., Patnaik, A., Singh, A., & Chauhan, S. C. (2018). Spectroscopic, microscopic characterization of Cannabis sativa leaf extract mediated silver nanoparticles and their synergistic effect with antibiotics against human pathogen. *Alexandria engineering journal*, *57*(4), 3043-3051.
39. Bhavi, S. M., Padti, A. C., Thokchom, B., Singh, S. R., Bhat, S. S., Bajire, S. K., ... & Yarajarla, R. B. (2024). Biogenic silver nanoparticles from Simarouba glauca DC leaf extract: Synthesis, characterization, and anticancer efficacy in lung cancer cells with protective effects in Caenorhabditis elegans. *Nano TransMed*, *3*, 100052.
40. Ali, M. H., Azad, M. A. K., Khan, K. A., Rahman, M. O., Chakma, U., & Kumer, A. (2023). Analysis of crystallographic structures and properties of silver nanoparticles synthesized using PKL extract and nanoscale characterization techniques. *ACS omega*, *8*(31), 28133-28142.
41. Mehta, B. K., Chhajlani, M., & Shrivastava, B. D. (2017, April). Green synthesis of silver nanoparticles and their characterization by XRD. In *Journal of physics: conference series* (Vol. 836, No. 1, p. 012050). IOP Publishing.
42. Desalegn, T., Murthy, H. A., & Limeneh, Y. A. (2021). Medicinal plant Syzygium guineense (willd.) DC leaf extract mediated green synthesis of Ag nanoparticles: investigation of their antibacterial activity. *Ethiopian Journal of Science and Sustainable Development*, *8*(1), 1-12.
43. Thiurunavukkarau, R., Shanmugam, S., Subramanian, K., Pandi, P., Muralitharan, G., Arokiarajan, M., ... & Shanmugam, V. (2022). Silver nanoparticles synthesized from the seaweed Sargassum polycystum and screening for their biological potential. *Scientific Reports*, *12*(1), 14757.
44. Shahzadi, S., Fatima, S., Shafiq, Z., & Janjua, M. R. S. A. (2025). A review on green synthesis of silver nanoparticles (SNPs) using plant extracts: a multifaceted approach in photocatalysis, environmental remediation and biomedicine. *RSC advances*, *15*(5), 3858-3903.
45. Mfon, R. E., & Amri, Z. A. (2023). Synthesis, Characterisation and Zeta Potential of Silver Nanoparticles. *American Journal of Sciences and Engineering Research*, *6*(1), 104-112.
46. Deepika, S., Selvaraj, C. I., & Roopan, S. M. (2020). Screening bioactivities of Caesalpinia pulcherrima L. swartz and cytotoxicity of extract synthesized silver

nanoparticles on HCT116 cell line. *Materials Science and Engineering: C*, *106*, 110279.

47. Jebril, S., Jenana, R. K. B., & Dridi, C. (2020). Green synthesis of silver nanoparticles using Melia azedarach leaf extract and their antifungal activities: In vitro and in vivo. *Materials Chemistry and Physics*, *248*, 122898.
48. Chowdhury, S. S., Ibnat, N., Hasan, M., & Ghosh, A. (2024). Medicinal Plant-Based nanoparticle synthesis and their diverse applications. In *Ethnopharmacology and OMICS Advances in Medicinal Plants Volume 2: Revealing the Secrets of Medicinal Plants* (pp. 213-250). Singapore: Springer Nature Singapore.
49. Dashora, A., Rathore, K., Raj, S., & Sharma, K. (2022). Synthesis of silver nanoparticles employing Polyalthia longifolia leaf extract and their in vitro antifungal activity against phytopathogen. *Biochemistry and Biophysics Reports*, *31*, 101320.
50. Khalil, S., Mehmood, A., Khan, M. A. R., Ahmad, K. S., Abasi, F., Raffi, M., ... & Abdelkarim, M. (2023). Antibacterial, antioxidant and photocatalytic activity of novel *Rubus ellipticus* leaf mediated silver nanoparticles. *Journal of Saudi Chemical Society*, *27*(1), 101576.
51. Abida, A., Almutairi, M. H., Mushtaq, N., Ahmed, M., Sher, N., Fozia, F., ... & Ullah, Z. (2023). Revolutionizing nanotechnology with Filago desertorum extracts: Biogenic synthesis of silver nanoparticles exhibiting potent antioxidant and antibacterial activities. *ACS omega*, *8*(38), 35140-35151.
52. Gurunathan, S., Han, J. W., Eppakayala, V., Jeyaraj, M., & Kim, J. H. (2013). Cytotoxicity of biologically synthesized silver nanoparticles in MDA-MB-231 human breast cancer cells. *BioMed research international*, *2013*(1), 535796.
53. Al-Asiri, W. Y., Al-Sheddi, E. S., Farshori, N. N., Al-Oqail, M. M., Al-Massarani, S. M., Malik, T., ... & Siddiqui, M. A. (2024). Cytotoxic and Apoptotic Effects of Green Synthesized Silver Nanoparticles via Reactive Oxygen Species–Mediated Mitochondrial Pathway in Human Breast Cancer Cells. *Cell Biochemistry and Function*, *42*(7), e4113.
54. Majid, A. (2025). Characterization, Antioxidant and Anticancer activities of Silver Nanoparticles using Serenoa repens. *Journal of Bioscience and Applied Research*, *11*(1), 37-49.
55. Zare-Bidaki, M., Nabavi Sales, F. S., Yousefinia, A., Mohammadparast-Tabas, P., Aramjoo, H., Torabi, M., ... & Ghoreishi, S. M. (2025). Exploring anticancer,

antifungal, antibacterial and antioxidant properties Colchicum luteum root-mediated silver nanoparticles with green synthesis. *Plasmonics*, *20*(7), 4589-4603.

56. Montazersaheb, S., Eftekhari, A., Shafaroodi, A., Tavakoli, S., Jafari, S., Baran, A., ... & Ahmadian, E. (2024). Green-synthesized silver nanoparticles from peel extract of pumpkin as a potent radiosensitizer against triple-negative breast cancer (TNBC). *Cancer Nanotechnology*, *15*(1), 47.
57. Alhajri, H., Alterary, S., Alrfaei, B. M., & Al-Qahtani, W. S. (2021). Therapeutic potential evaluation of green synthesized silver nanoparticles derived from olive (Olea europaea L.) leaf extracts against breast cancer cells. *Journal of Nanophotonics*, *15*(3), 036003-036003.
58. Bin-Jumah, M., Al-Abdan, M., Albasher, G., & Alarifi, S. (2020). Effects of green silver nanoparticles on apoptosis and oxidative stress in normal and cancerous human hepatic cells in vitro. *International journal of nanomedicine*, 1537-1548.
59. Takáč, P., Michalková, R., Čižmáriková, M., Bedlovičová, Z., Balážová, Ľ., & Takáčová, G. (2023). The role of silver nanoparticles in the diagnosis and treatment of cancer: are there any perspectives for the future?. *Life*, *13*(2), 466.
60. Raja, G., Jang, Y. K., Suh, J. S., Kim, H. S., Ahn, S. H., & Kim, T. J. (2020). Microcellular environmental regulation of silver nanoparticles in cancer therapy: a critical review. *Cancers*, *12*(3), 664.
61. Faheem, M. M., Bhagat, M., Sharma, P., & Anand, R. (2022). Induction of p53 mediated mitochondrial apoptosis and cell cycle arrest in human breast cancer cells by plant mediated synthesis of silver nanoparticles from Bergenia ligulata (Whole plant). *International journal of pharmaceutics*, *619*, 121710.
62. Pandey, P., Lakhanpal, S., Bishoyi, A. K., Jyothi, S. R., Mishra, S., Verma, M., ... & Khan, F. (2025). Biosynthesis of silver nanoparticles from plant extracts: a comprehensive review focused on anticancer therapy. *Frontiers in Pharmacology*, *16*, 1600347.
63. Wani, A. K., Akhtar, N., Mir, T. U. G., Singh, R., Jha, P. K., Mallik, S. K., ... & Prakash, A. (2023). Targeting apoptotic pathway of cancer cells with phytochemicals and plant-based nanomaterials. *Biomolecules*, *13*(2), 194.
64. Majtnerová, P., & Roušar, T. (2018). An overview of apoptosis assays detecting DNA fragmentation. *Molecular biology reports*, *45*(5), 1469-1478.
65. Cao, K., Riley, J. S., Heilig, R., Montes-Gómez, A. E., Vringer, E., Berthenet, K., ... & Tait, S. W. (2022). Mitochondrial dynamics regulate genome stability via

control of caspase-dependent DNA damage. *Developmental cell*, *57*(10), 1211-1225.

66. Kari, S., Subramanian, K., Altomonte, I. A., Murugesan, A., Yli-Harja, O., & Kandhavelu, M. (2022). Programmed cell death detection methods: a systematic review and a categorical comparison. *Apoptosis*, *27*(7), 482-508.
67. Irani, N., Sadat Shandiz, S. A., Yousefi, V., & Davoodi-Dehaghani, F. (2025). Green synthesis of silver chloride nanoparticles derived from Artemisia sieberi extract (AgClNPs-ASE) induces cell cycle arrest and triggers apoptosis in human breast (MDA-MB-231) cancer cells. *Inorganic and Nano-Metal Chemistry*, *55*(5), 527-541.
68. Habeeb Rahuman, H. B., Dhandapani, R., Narayanan, S., Palanivel, V., Paramasivam, R., Subbarayalu, R., ... & Muthupandian, S. (2022). Medicinal plants mediated the green synthesis of silver nanoparticles and their biomedical applications. *IET nanobiotechnology*, *16*(4), 115-144.
69. Pushparaj, K., Balasubramanian, B., Kandasamy, Y., Arumugam, V. A., Kaliannan, D., Arumugam, M., ... & Meyyazhagan, A. (2023). Green synthesis, characterization of silver nanoparticles using aqueous leaf extracts of Solanum melongena and in vitro evaluation of antibacterial, pesticidal and anticancer activity in human MDA-MB-231 breast cancer cell lines. *Journal of King Saud University-Science*, *35*(5), 102663.
70. Yesilot, S., Bayram, D., Özgöçmen, M., & Toğay, V. A. (2023). Apoptotic effects of Phlomis armeniaca mediated biosynthesized silver nanoparticles in monolayer (2D) and spheroid (3D) cultures of human breast cancer cell lines. *3 Biotech*, *13*(1), 4.
71. Joseph, J., Khor, K. Z., Moses, E. J., Lim, V., Aziz, M. Y., & Abdul Samad, N. (2021). In vitro anticancer effects of Vernonia amygdalina leaf extract and green-synthesised silver nanoparticles. *International Journal of Nanomedicine*, 3599-3612.
72. Hosseini, S. M., Soleimani, A., Khaleghi, S., & Hajrasouliha, S. (2024). Green synthesized ag nanoparticles as promising antibacterial and antitumor agents: in vitro studies. *Indian Journal of Microbiology*, 1-15.
73. Liu, Y., Ren, S., Sang, Q., Cheng, X., & Bi, Y. (2025). Potential Active Compounds of Ganoderma lucidum and Their Anticancer Effects: A Comprehensive Review. *Food science & nutrition*, *13*(8), e70741.

74. Takáč, P., Michalková, R., Čižmáriková, M., Bedlovičová, Z., Balážová, Ľ., & Takáčová, G. (2023). The role of silver nanoparticles in the diagnosis and treatment of cancer: are there any perspectives for the future?. *Life*, *13*(2), 466.
75. Mishra, V., Nayak, P., Singh, M., Tambuwala, M. M., Aljabali, A. A., Chellappan, D. K., & Dua, K. (2021). Pharmaceutical aspects of green synthesized silver nanoparticles: A boon to cancer treatment. *Anti-Cancer Agents in Medicinal Chemistry-Anti-Cancer Agents)*, *21*(12), 1490-1509.
76. Vallinayagam, S., Rajendran, K., & Sekar, V. (2021). Green synthesis and characterization of silver nanoparticles using Naringi crenulate leaf extract: key challenges for anticancer activities. *Journal of Molecular Structure*, *1243*, 130829.
77. Asadi, M., Taghizadeh, S., Kaviani, E., Vakili, O., Taheri-Anganeh, M., Tahamtan, M., & Savardashtaki, A. (2022). Caspase-3: structure, function and biotechnological aspects. *Biotechnology and Applied Biochemistry*, *69*(4), 1633-1645.
78. Kim, C. G., Castro-Aceituno, V., Abbai, R., Lee, H. A., Simu, S. Y., Han, Y., ... & Yang, D. C. (2018). Caspase-3/MAPK pathways as main regulators of the apoptotic effect of the phyto-mediated synthesized silver nanoparticle from dried stem of Eleutherococcus senticosus in human cancer cells. *Biomedicine & Pharmacotherapy*, *99*, 128-133.
79. Plackal Adimuriyil George, B., Kumar, N., Abrahamse, H., & Ray, S. S. (2018). Apoptotic efficacy of multifaceted biosynthesized silver nanoparticles on human adenocarcinoma cells. *Scientific reports*, *8*(1), 14368.
80. Montazersaheb, S., Farahzadi, R., Fathi, E., Alizadeh, M., Amir, S. A., Ardakan, A. K., & Jafari, S. (2024). Investigation the apoptotic effect of silver nanoparticles (Ag-NPs) on MDA-MB 231 breast cancer epithelial cells via signaling pathways. *Heliyon*, *10*(5).